



Critical behaviour of seismic systems and dynamics in ensemble of strong earthquakes

Samvel Ts. Akopian¹ and Armen N. Kocharyan²

¹ Schmidt Institute of Physics of the Earth, Gruzinskaya str., 10-1 Moscow 123995, Russia

² Department of Physics and Astronomy, California State University Los Angeles, CA 90032, USA. E-mail: armen.kocharyan@calstatela.edu

Accepted 2013 September 27. Received 2013 September 15; in original form 2012 November 2

SUMMARY

We present the basic regularities that govern the time evolution dynamics of earthquakes in the seismic system (SS) defined as a unique active volume of lithosphere responsible for preparation of strong earthquakes above a certain threshold magnitude. This concept was articulated previously within phenomenological approach of seismic entropy which utilizes real-time monitoring of strong earthquakes. Seismic parameters such as cumulative energy, number of seismic system states and entropy are calculated to reliably describe in real space–time the non-equilibrium dynamics of the active volume of the Earth's lithosphere. The behaviour of seismic parameters also shows the direction of tectonic processes which preserve a long-term memory of all previously released energies of preceding earthquakes as well as the time when they occurred. The obtained power-law relationship between the information entropy and cumulative energy within a cycle implies that seismically ideal homogeneous system over time tends to the certain critical conditions (attractor). The well-defined SS forms an ensemble of strong earthquakes with critical instabilities which periodically restore the equilibrium state of the system. The finite size of SS and minimal unit of microquake leads to selectivity and discreteness of the earthquake magnitude. It is found that indicator earthquakes above certain threshold magnitudes at which the Gutenberg–Richter law is often violated, play a crucial role in preparation of strong earthquakes. The calculated trajectory diagrams describing the dynamic evolutions of lithosphere allow construct the attractor for real SSs by solving the inverse problem.

Key words: Instability analysis; Inverse theory; Probability distributions; Seismic cycle; Earthquake dynamics; Statistical seismology.

1 INTRODUCTION

The major structural elements of the lithosphere activities relevant to stress-strength fields are inaccessible to direct measurement. The problem of the practical forecast of earthquakes can be solved by integration of various methods and approaches which involve different types of observational data. Here we consider the complex problem of strong earthquake preparation and forecasting theoretically based on the statistical interpretation of seismic data. Although the preparation of strong earthquakes differs from case to case, a common pattern of seismic behaviour in the geological medium that is responsible for strong earthquake preparation can be analysed by looking at the dynamic responses of preceding earthquakes to non-equilibrium dissipative processes. In a recent review (Jordan *et al.* 2011), current methods of forecasting and predicting earthquakes are reduced to the study of fault slip events which supposedly may occur for a specified magnitude range in a given space–time domain. It also mentions that, in most cases, the spatial domain is considered to be a contiguous geographic region consisting of

the seismogenic volume of the lithosphere. However, this approach leaves uncertainty in the selection of the appropriate active volume for studying the processes which lead to strong earthquakes. This uncertainty is due to the lack of a unified scenario for strong earthquake preparation which extends consecutively through all stages of the dissipative and non-dissipative processes that occur in a given geological medium.

A unified approach is used to estimate the probability of large earthquakes occurring within the San Andreas Fault (SAF) system in California (Field *et al.* 2009). The seismically active volume of lithosphere responsible for the preparation of a certain energy class of earthquakes is key in determining complex earthquake dynamics (Akopian 1995a, 1998a). We call this specific volume of the lithosphere the ‘seismic system’ (SS). The preparation of earthquakes at different ranges of magnitude is ultimately tied to the hierarchy of SSs. There are different scales of discrete volumes of geological media. Our model of the selectivity and discreteness of media volumes and earthquake magnitudes differs from the conventional view, which considers these values to be continuous variables. These

discrete volumes provide upper threshold magnitudes which naturally divide earthquakes into strong and relatively weak indicator earthquakes. Indicator earthquakes provide information about the energy states of the lithosphere and about the deviation of the SS from equilibrium. When the total released energy in the SS is insufficient to restore balance, the system enters a critical (unstable) phase and undergoes a transition to equilibrium, culminating in a strong earthquake.

In theories of self-organized criticality (Bak & Tang 1989; Barriere & Turcotte 1994; Rundle *et al.* 2000) the selective properties of a medium, such as the discrete magnitude of earthquakes or its finite volume, are often ignored. The introduction of entropy in seismology based on the Gutenberg–Richter (GR) empirical law (Gutenberg & Richter 1954) is commonly used to study dynamic systems and the macroscopic behaviour of seismicity (Main & Al-Kindy 2002; Al-Kindy & Main 2003; Main & Naylor 2010). Due to uncertainty in the selection of space and volume, the GR law leaves this freedom of choice to each individual seismologist. Entropy is also determined according to the GR law for arbitrary space–time intervals (De Santis *et al.* 2011). This concept has been successfully used in relation to the source region and to the foreshock and aftershock time intervals of recent earthquakes in central Italy. The dynamics of earthquake sequences in sliding time windows before and after strong earthquakes are also analysed. However, the GR law is unsuitable to accurately describe seismic activity because it averages the time and magnitude of earthquakes and arbitrariness in the selection of volumes. Additionally, this empirical law seems to be violated at large earthquake magnitudes (Kagan 2000). Relatively weak earthquakes are statistically well described by the GR law because their high frequency results in small energy contributions being made to the dynamic processes involved.

In our approach we use entropy as defined by Akopian (1995a) without time averaging or disturbing the actual chronology of events. Crucially, our approach also includes definitions for studying areas and the current moment in time because it describes the state of the geological medium between seismic events. For mathematical modelling of seismic processes we introduced a metric, the number of SS states and information entropy. This enables us to identify the law of maximal probability for the system state, where equilibrium is restored by the occurrence of a strong earthquake. This law allows one to determine the volume of the SS and the threshold magnitudes of indicator earthquakes. One can also monitor strong earthquakes at all stages of preparation (long, middle and short) within chosen time intervals (seismic cycles).

Alternatively, cumulative energy and seismic entropy can be considered to be the most suitable integral characteristics of seismic behaviour at any given time. Cumulative energy and the total number of system states over time can also be analysed on the basis of the released energies of indicator earthquakes. Threshold magnitudes, the time intervals of seismic cycles and cumulative parameters are all manifestations of phase instability and constitute critical behaviour of seismically homogeneous or inhomogeneous structures. The volume of SS usually occupies a much larger space, one which includes the sources of ensembles of strong earthquakes. The faulting involves non-linear processes which are highly sensitive to immeasurably fine details that occur throughout a large volume of space, not just in the immediate vicinity of the hypocentre (Geller 1997). The parameters of the system states within the seismic cycle play a key role in the dynamics of the long-term behaviour of the system. Furthermore, the SS responsible for the preparation of strong earthquakes can be defined statistically only when they form a canonical ensemble of (statistically) independent seismic events

(Landau & Lifshits 1980; Prigogine 1980). Thus, we introduce the concept of a strong earthquake population, that is, an ‘ensemble’ with an ‘independent’ set of subsystems for the same volume of geological medium which occur at different time intervals (seismic cycles). This concept, which differs from the dynamics of the SS within a single cycle, is extremely useful for the statistical consideration of earthquake processes in real space–time.

A key formulation of statistical mechanics in terms of information theory is given using the Gibbs algorithm (Jaynes 1979). Information entropy governs the dynamics of non-equilibrium processes which are crucial for understanding complex system behaviours (Anderson 1991). In seismology this approach uses information entropy theory to describe the space–time dynamics of non-equilibrium processes for seismically inhomogeneous geological structures (Rivera & Kanamori 2002). The theory can be constructed directly in terms of space paths that maximize the information entropy probability summed over all the permitted microscopic states (Dewar 2003). The maximum-entropy production principle can also be used to predict the quasi-stationary properties of a generally open non-equilibrium system exchanging energy and mass with its surrounding medium.

This paper establishes the central relationship between cumulative energy and entropy functions in describing the clustering of strong earthquakes into attractors which form a canonical ensemble and are part of SS dynamics. Our approach treats the seismically active geological medium as an open dissipative system away from its equilibrium. The concept of information entropy is used to measure missing information from the SS, which is undergoing non-equilibrium dynamic processes. Discussion is limited to the description of ensembles of strong earthquakes on a long timescale (slow time preparation) when random indicator earthquakes eventually start to cooperate and give rise to critical behaviour prior to strong earthquakes.

After introducing various aspects of earthquake dynamics, SS states and the seismic entropy method are defined in Section 2. The long-time evolution of the (primary) ideal homogeneous system, which is driven by the power law, the development of earthquake instabilities and the formation of spatially inhomogeneous structures, is considered in Section 3. Information entropy is used to formulate criteria for critical behaviour in an ensemble of strong earthquakes, which forms a specific attractor on the trajectory diagram. The results obtained for an ideal homogeneous SS can also be applied to a real system. The inverse method is applied to illustrate the parameters of an attractor for a number of real systems. These questions are considered in Section 4. Concluding remarks are given in Section 5. The obtained results are illustrated by example of SS Sakhalin in Appendix A and the maps for configuration and zones of instabilities in the real SSs are shown in Appendix B.

2 METHOD

2.1 Seismic system

These are the basic principles which underlie the developed method (Akopian 1995a,b, 1998a). Consider a seismically active region of external compression with the plate tectonic positions. The lithosphere in the active regions has a complicated plate-block hierarchic structure with specific seismic properties. To model this structure we introduce a number of parameters and definitions. Each earthquake can be described by a vector with characteristic time–space and energy coordinates $\phi_i, \lambda_i, h_i, t_i, E_i$, with a latitude ϕ_i , a longitude λ_i , a focal depth h_i and a time t_i when an earthquake occurs. A radiated

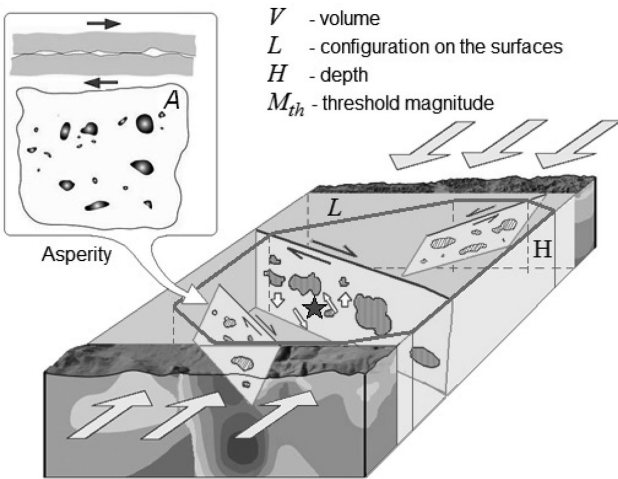


Figure 1. A schematic illustration of a hypothetical seismic system with surface configuration L , depth H and planes of active faults (asperities) with contact areas A under an external compression.

seismic energy E_i is determined by the earthquake magnitude M_i (Gutenberg & Richter 1956):

$$\log E_i = \alpha + \gamma M_i, \quad (1)$$

in terms of $\alpha = 4.8$ and $\gamma = 1.5$ parameters, where energy is measured in Joules. The spatial location of a rupture is usually the point at the hypocentre depth on a fault where the rupture has been nucleated at the time of its first dynamic motion. The accepted (simplified) model of an earthquake, a point source of radiated seismic energy in space, is sufficient to solve the problems raised in this paper. Therefore, volume characteristics of the source (faulting, focal mechanisms, and so on) are neglected.

The SS is a large-scale formation which may include segments of active faults that can potentially generate strong earthquakes. The SS is defined as an enclosed volume V of lithosphere where strong earthquakes are prepared. This volume includes not only the strong earthquake's sources but also a much wider area of lithosphere. The SS is schematically depicted in Fig. 1, which shows section and plane views of the real contact areas (asperities) on the surfaces of faults (Scholz 1990; Johnson 2010). The characteristic parameters of an SS are also shown in the figure. Our ultimate goal is to find the correct boundaries of SS volume (depth H and configuration on the surfaces L). The initial volume of SS is selected on the basis of the plate tectonic model of the region. Boundaries are then specified using the new seismic regularities. The SS is also characterized by a threshold magnitude M_{th} . All earthquakes with magnitudes greater than or equal to the threshold $M \geq M_{th}$ are called strong and earthquakes with magnitudes $M_{min} \leq M < M_{th}$ are considered to be indicator earthquakes, where M_{min} is the minimal value among all representative earthquakes in a regional catalogue.

The time interval between two successive strong earthquakes in the SS, $T_j = t_j - t_{j-1}$, is labelled a seismic cycle, where t_j and t_{j-1} denote the times when two consecutive strong earthquakes occur. Hereafter, all the varying parameters within the seismic cycles are denoted by the subscript i , while the seismic cycles are numbered by j ($j = 1, 2, \dots, N$), where N is the number of realized seismic cycles, that is, the number of strong earthquakes. The current time interval T within any seismic cycle j is equal to $T = t - t_{j-1}$, with t_0 being the starting date of the first cycle. The quantitative description of seismic processes (or mathematical modelling) in the defined SS establishes a functional relationship between the

parameters of strong earthquakes and the cumulative parameters for indicator earthquakes. The larger the number of completed seismic cycles (in an ensemble of strong earthquakes) in a given SS, the more the results are (statistically) accurate.

2.2 Seismic system states

We now present the main principles for mathematically modelling seismic processes in the SS. This requires catalogue data of representative earthquakes with $M \geq M_{min}$ and the preliminary plate tectonic model of the region. The time interval δt for actual calculations is taken as a single unit of time, that is, a second, minute, hour, month and so on. Suppose that $N - 1$ cycles were accomplished at time t starting from some initial date of observation t_0 . The total released energy in the SS within seismic cycles (after each strong earthquake) is defined by the parameter of cumulative energy E_c , which is equal to the total radiated energy of all indicator earthquakes registered up to any given time, t (Fig. 2):

$$E_c(t) = \sum_{i=1}^{\tilde{N}(t)} E_i, \quad (2)$$

where a summation includes all indicator earthquakes $\tilde{N}(t)$ for a given time t with energies $E_i \geq E_{min}$ in a volume V of SS as recorded after the last strong earthquake t_{N-1} . Below, the spatial characteristics of indicator earthquakes in the SS volume are omitted for simplicity. The scheme of calculation $E_c(t)$ is shown in Fig. 2 after the occurrence of a hypothetical strong earthquake at time t_0 . A similar cumulative parameter for the total seismic energy was introduced in a slightly different formulation by Tsuboi (1965).

For time description of the system state a new parameter $S_N(t)$ is introduced, which is analogous to action in Newtonian mechanics:

$$S_N(t) = (t - t_{N-1})E_c - \sum_{i=1}^{\tilde{N}(t)} (t_i - t_{N-1})E_i, \quad (3)$$

where t_i and E_i are the indicator earthquake occurrence time and radiated seismic energy, respectively. The parameter t_{N-1} is the time

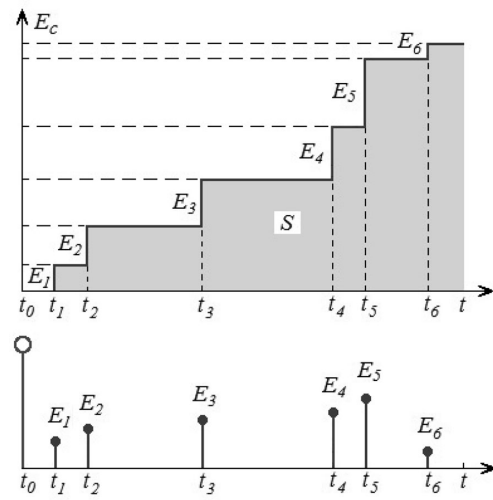


Figure 2. A schematic picture of a stepwise increase of the cumulative energy $E_c(t)$ function versus time within the first seismic cycle, beginning from time t_0 of a hypothetical strong earthquake. The energy values E_i and corresponding time occurrences t_i ($i = 1-6$) of the six indicator earthquakes are also shown. The parameter $S(t)$ is equal to the total area beneath the cumulative energy function $E_c(t)$.

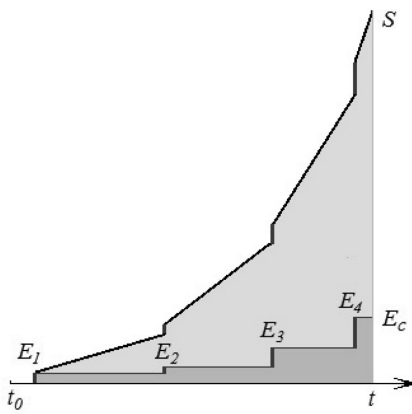


Figure 3. The rapid growth of the parameter $S(t)$ is compared to the step-like increase of the cumulative energy, $E_c(t)$. The cumulative energy controls the rate of change of $S(t)$ in time, and any new indicator earthquake leads to a slope increase.

of occurrence of the last strong earthquake event. The expression (3) at current time $T = t - t_{j-1}$ within any cycle j can be reduced to the more compact form:

$$S = TE_c - \sum_{i=1}^N T_i E_i. \quad (4)$$

Mathematically, (integral) parameter $S(t)$, as shown in Fig. 2 describes the area beneath the cumulative energy function $E_c(t)$ plotted versus time. Fig. 3 illustrates the comparative behaviour of the SS parameters $E_c(t)$ and $S(t)$. The seismic parameter $S(t)$ shows significant rapid growth in comparison with the step-like increase of cumulative energy. The cumulative parameter $E_c(t)$ controls the rate change of $S(t)$, and any new indicator earthquake inevitably leads to an increase in the slope of the function $S(t)$. Therefore, both the $S(t)$ and $E_c(t)$ parameters are non-descending functions of time. For convenience, to avoid the complications caused by large numbers in seismology, we substitute for (2) and (3) the corresponding decimal logarithmic scales:

$$K_c(t) = \log E_c(t), \quad W(t) = \log S(t), \quad (5)$$

where K_c is defined as the cumulative energy class of indicator earthquakes and W has meaning in seismic entropy analogous to the physical entropy in thermodynamics. The cumulativeness keeps the time memory of past behaviour and the sequence order of past earthquake events. In practice, these parameters are very reliable and can easily be calculated on the basis of earthquake data provided by existing catalogues. Therefore, at any time within the seismic cycle, the state of the SS is determined by the pair of parameters E_c and S (or K_c and W). The graphs of parameters E_c and W in the seismic cycles of the SS Sakhalin are shown in Appendix A. The physical meaning of these parameters is discussed in the next sections.

2.3 Seismic entropy

Time-dependent cumulative energy (2) has a very transparent physical meaning. The non-decreasing function E shows the direction flow of seismotectonic processes in volume V with a time; it also preserves the memory of all the released elastic seismic energy. The parameter S in eq. (3) keeps memory information about the amount of radiated (elastic) energy and the time occurrences of indicator earthquakes. The essential point here is that, even during seismic quiescence, when the cumulative seismic energy E_c

practically remains constant, the parameter $S(t)$ of the system still linearly increases with time. This means that, in the absence of seismic activity, the parameter S gathers important information about the dynamic behaviour of the system structure. Therefore, the longer the observation time, the more information is obtained. Indirectly, the parameter S contains common information about the elastic and inelastic processes occurring in a given volume V of seismogenic medium over time.

The behaviour of the system depends on the processes that occur at contact surface irregularities (faults) under external compression. Faulting, creeping, fluid flow, microcracks, weakening and strengthening, more than other things which take place in the local domains of systems (but not necessarily in earthquake source zones), are complex irreversible processes that occur in systems over time. These processes, which act collectively, describe the dynamic behaviour of an open dissipative SS. From one side, the parameter S keeps memory about total radiated energy of indicator earthquakes. From the other, S specifies the quiescent time evolution of the SS between seismic activities. The function S in (3) contains both space-time and energy information about the SS medium. As shown below, this function may play a key role in describing seismic processes.

To mathematically model the SS at different levels (from the microscopic to the macroscopic), an appropriate metric is introduced: the ‘minimal’ informational unit for the seismic state scale. Estimates of the parameters of all earthquakes from microfractures (nanoequakes) to major earthquakes have been made (Scholz 1968; Teng & Henyey 1981; Mogi & Mochizuki 1983; Molnar *et al.* 2007). We select a unit of microscopic energy for an earthquake, E_h , which uniquely defines the corresponding unit (elementary) volume of source V_h and its linear (rupture) size l_h :

$$V_h = \frac{E_h}{\epsilon} \quad l_h = (V_h)^{1/3}, \quad (6)$$

where

$$\epsilon = 10^{-4} \text{ J cm}^{-3} \quad (7)$$

is the maximal available density of potential energy in rocks that are under limiting deformation (Tsuboi 1956). There is an attempt to systematize (classify) small seismic events into categories: microfracture or nanoequakes, microearthquakes and weak earthquakes (Levin *et al.* 2010). For a quantitative description of the seismic process, it is important to choose the weakest seismic microearthquake energy, that is, $E_h = 1 \text{ J}$. The magnitude of such an elementary quake is equal to $M_h = -3.2$. The linear size is $l_h \approx 22 \text{ cm}$, the faulting time is $\delta t_h \ll 1 \text{ s}$, and the duration of the signal is $< 1 \text{ s}$. The metric unit of time is defined as a minimal (measurement) time interval, which can be taken to be $\delta t = 1 \text{ s}$. This overestimated accuracy (which is practically unattainable) is quite sufficient to describe the time evolution of real seismic processes with high precision (Kanamori 2004). Limited by this time interval, we obtain an elementary (action) parameter h_s for the weakest seismic microearthquake of energy $E_h = 1 \text{ J}$ in the SS registered in 1 s (Akopian 1995a):

$$h_s = 1 \text{ J s}. \quad (8)$$

This action involves a unit (elementary) source of volume for the microearthquake $V_h \approx 10^4 \text{ cm}^3$, which is needed to generate a minimum amount of seismic radiation energy equal to 1 J. The minimal basic unit (quake) measures the scale of space-energy inhomogeneity in the system. In practice, the choice of an elementary portion of seismic energy is determined by the level of seismic noise, the

sensitivity of seismic instruments, and the system size. In studying the ‘rock-crush’ under laboratory conditions and when solving problems of soil mechanics based on our approach, the elementary parameter (8) may be taken as a much smaller value.

Entropy as a measure of disorder is a fundamental concept for the characterization of complexity dynamics of natural processes which can also be applied to earthquakes. By analogy with the physical entropy in thermodynamics (Landau & Lifshits 1980), the introduction of cumulative parameter W in the logarithmic scale (5) defines seismic entropy:

$$W = \log \frac{S}{h_s}, \quad (9)$$

where, as shown below, the dimensionless parameter S/h_s gives the number of total energy states available to the SS during the time elapsed since the most recent strong earthquake. It is apparent that W is zero for $S = h_s$, which corresponds to the minimal energy portion of the basic state (1 J). The SS in this basic state (at an initial stage of evolution) is defined as ideally homogeneous. Thus, the initial ideal SS can only have spatial inhomogeneities (cracks) that are smaller than the basic elementary unit crack. For simplicity, everywhere below we use dimensionless parameters $S/h_s \rightarrow S$, $E_c/E_h \rightarrow E_c$, $t/\delta t \rightarrow t$. The subscript c of cumulative energy can be omitted for simplicity, unless otherwise stated.

2.4 Degenerate seismic states

As postulated in earlier papers (Akopian 1995a, 1998a), the function S equals the total number of possible states of a system within a seismic cycle, which is demonstrated as follows. Formally, an elementary state of the SS consists of a cell with the dimensionless value, $S = 1$. Let us call this basic quake (BQ), with a minimum energy state and zero entropy ($W = 0$), an ideal seismically homogeneous equilibrium state. Note that BQ is a metric (unit) of the cumulative energy of indicator earthquakes and of parameter S . For example, if the cumulative energy per unit time increases by three BQ, it implies that one indicator earthquake has energy equal to three BQ (the number of BQ is not equal to the number of indicator earthquakes). We also assume, for simplicity, that in such an ideal homogeneous system, indicator earthquakes occur randomly and without accompanying noise. For $S = 1$, the system has only a single BQ state which has a single energy, $E = 1$. Next, consider $S = 2$ which implies a system with two cells, that is, the system that can exist in either of two states with different energies, $E = 1$ and 2. The $E = 1$ energy state exists for the two successive (time) intervals, while $E = 2$ state with two BQ energies exists in the second time interval. For $S = 3$, there are three cells (states) with three possible cumulative energies, $E \leq S$: the $E = 1$ state corresponds to one BQ energy for the three successive intervals; the $E = 2$ state corresponds to one BQ energy for the second and two BQ energy for the third time intervals; the $E = 3$ state is three BQ energy units in the third time interval. These three states have different values of cumulative energy E . For $S = 4$, there are four final states of the system, with cumulative energies of $E = 1, 2, 3$ and 4, respectively. However, as you can see from Fig. 4, the state with $S = 4$ and $E = 2$ becomes degenerate, since there are two final states with energy $E = 2$. Here, we call the state degenerate, since for a given S , the system arrives to its final state with the same E by two or more different paths. For $S = 5$, we find five energy states of the system. States with $E = 1, 4$ and 5 are non-degenerate, while both final states with $E = 2$ and 3 are double degenerate. For $S = 6$, the system has six states. States with $E = 2, 3$ are triple degenerate, and the $E = 4$ state is double de-

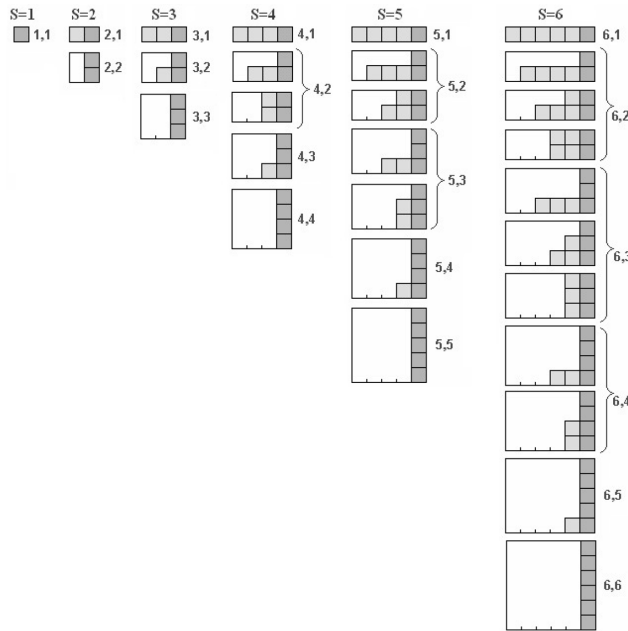


Figure 4. All possible cumulative energy states of a system with $S = 1\text{--}6$. One elementary (square) cell is described by a basic quake unit measured in units of 1 J s. On the right-hand side of each column, corresponding quantities of various cumulative energies E for given values of S are denoted by (S, E) . States with $S \leq 3$ are non-degenerate; state degeneracy increases with $S \geq 4$. The number of degenerate states is shown in curly brackets. Dark squares denote final states for each S value.

generate. All these states, up to $S = 6$, are shown in Fig. 4. Detailed examination at the cell level shows that, for any given S value, the number N of all possible final cumulative energy states of the SS is always equal to S ($N = S$). These final states ($N = S$) in Fig. 4 are denoted by dark squares.

Any current (final) state of the SS can be presented by a point $q_i = q(S_i, E_{ci})$ on a trajectory diagram $\{S, E_c\}$. The step-like path connecting the origin with a current state is called a trajectory. Each jump-like (path) interval seen on the trajectory diagram in Fig. 4 corresponds to an indicator earthquake. Also, the number n of all possible paths (trajectories) to the final state for $S > 3$ is greater than N ($n > N$), because some of the states are degenerate. The number of degenerate states increases gradually with increasing S . The degree of degeneracy (m_i) of a current state depends on the number of possible trajectories m_i which can lead a system to its final state. It is obvious that

$$\sum_{i=1}^S m_i = n. \quad (10)$$

For the random events considered here, all discrete values of cumulative energy $E \leq S$ are available to the SS. So, if we look at the energy states of the system (Fig. 4) without taking into account all possible paths which can lead to this final condition, then all the cumulative energy states have an equal probability. However, the past seismic history of energy release (an indispensable prerequisite for cumulative energy) can be of great importance in the earthquake. Therefore, for a given S , degenerate cumulative energy states actually have a higher number of possible final states and are more probable. Entropy (9) describes the energy state of an SS in the absence of degeneracy ($N = S$), when information about the number of trajectories is fully abandoned. We next determine information

entropy in a SS using the probability distribution of random seismic events in various energy states.

3 CRITICAL BEHAVIOUR OF SS

3.1 Information entropy

Suppose there is a discrete and finite set of SS states with various cumulative energies E_{ci} , where $i = 1, 2, \dots, S$ (S is the number of possible energy states of the SS). To distinguish between discrete values of the cumulative energy $E_c(t)$ and the energy E_i of indicator earthquakes, we introduce the notation E_{ci} . For each fixed S , these states differ by the values represented by the cumulative energy E_{ci} . To include a possible degeneracy (10) and view indicator earthquakes as totally random events, we introduce the probability p_i of detecting the SS in states with various cumulative energies E_{ci} :

$$p_i = \frac{m_i}{n}, \quad \text{where } 0 < p_i < 1, \quad \sum_{i=1}^S p_i = 1. \quad (11)$$

Here, the microstate probabilities p_i , in conformance with relevant external tectonic constraints that act on the system, describe the geological medium using the theoretical tools of microcanonical, canonical and grand-canonical distributions for isolated, closed and open systems, respectively (Pathria 2005). Using the (probability) frequency p_i of occurrences E_{ci} , we define the mean cumulative energy $\langle E \rangle$ of indicator earthquakes (Kolmogorov *et al.* 1982):

$$\langle E \rangle = \sum_{i=1}^S p_i E_{ci}. \quad (12)$$

The time evolution of earthquakes is a typical example of non-equilibrium irreversible processes characterized by an energy transformation that includes an increase in both thermodynamic entropy and information entropy. By analogy with Shannon entropy (Shannon 1948; Haken 1978; Nicolis & Prigogine 1989), we define seismic information entropy as

$$\langle W \rangle = - \sum_{i=1}^S p_i \log(p_i), \quad (13)$$

where distribution p describes the most probable cumulative energy states of indicator earthquakes in volume V at any given time. However, in seismology it is more appropriate to use the decimal logarithm base instead of the binary one which is used in Shannon entropy. Physical entropy converts to dimensionless seismic entropy by means of the conversion factor $1/(k \ln 10) = 0.315 \times 10^{23}$ (K J⁻¹), where k is the Boltzmann constant (Nicolis 1986). Conversion from dimensionless seismic entropy to dimensionless information entropy (in bits) is achieved by using through the factor $1/\log 2 = 3.322$ (bits). In other words, seismic and information entropies are almost equivalent and differ from the thermodynamic characteristics of geological media. Substituting (11) into expression (13), we find

$$\langle W \rangle = \log n - \frac{1}{n} \sum_{i=1}^S \{m_i \log(m_i)\}. \quad (14)$$

From (13) we find, that for a strongly ordered system such as an attractor, $p_i = 1$ for one possible value of i and $p_i = 0$ for all other values of i . This corresponds to the SS state after the culmination of a strong earthquake, when it has zero uncertainty in information entropy, $\langle W \rangle = 0$, that is, there is complete (maximum) information about the SS. For the uniform distribution $p_i = \tilde{p} = 1/S$

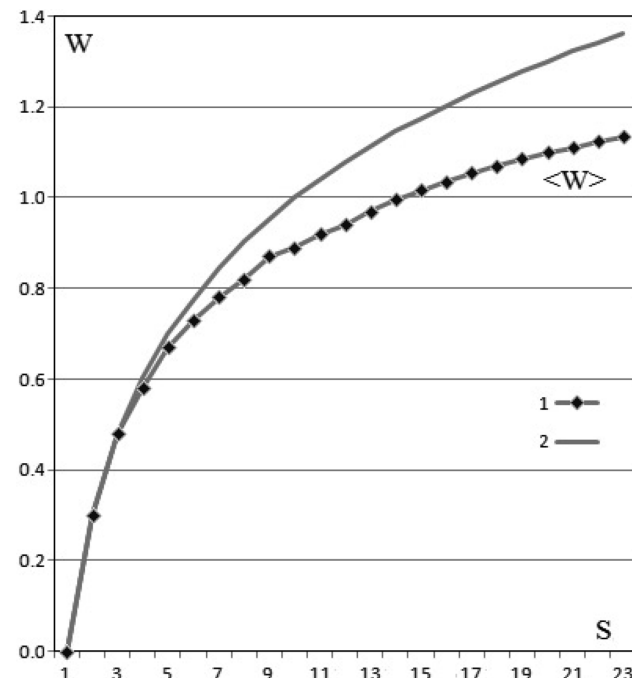


Figure 5. The calculated information entropy increase for: (1) a degenerate case; (2) a uniform distribution of probability. The rate of entropy increase in case of degeneracy with a lower number of probable states is smaller.

(without degeneracy), the amount of information required to completely determine the SS state equals $\langle W \rangle_{\max} = \log S$. Apparently, the maximum information entropy or state of maximum uncertainty (13) corresponds to the entropy of a (chaotic) SS (9). Eq. (14) is transformed into (9) when $m_i = 1$, that is, in the absence of degeneracy. Fig. 5 shows the variation in information entropy $\langle W \rangle$, with S ranging from 1 to 23, for two curves: one curve shows a uniform probability distribution and the other one shows degeneracy. Degeneracy between these two curves begins at $S > 3$. The degeneracy of energy states reduces the number of probable states and makes the prediction of an outcome more accurate. As a result, the rate of entropy increases as degeneracy decreases.

3.2 Seismic (state) probability

We next study in greater detail a non-uniform probability distribution involving degeneracy (11). Using Pascal's triangle as a model (Kolmogorov *et al.* 1982), we construct a triangle matrix for the appropriate number of SS states Fig. 6. In this triangle, each matrix element represents the number of possible trajectories to each destination in the current SS state (S_i, E_{ci}). Columns and rows in matrix are denoted by S and E_c , respectively. The Pascal's triangle matrix elements for SS are shown for S and E_c values that range from 1 to 12. The first column and two rows of diagonal matrix elements are equal to 1. At the beginning of a seismic cycle, a system with small E and S values has path trajectories that start in the vicinity of the diagonal, that is, in an equilibrium state, with $E = S$. In real systems, only a weak frequent seismicity results in no change of equilibrium state. A system can remain in such a condition for quite a long time (many thousands of years) before its tectonic situation changes. Such patterns are observed within plate areas far from boundaries, and in creep zones.

Fig. 7 shows two different occurrences: frequent ($E = S$) and relatively rare ($E < S$) seismic activity, near and far from the

E_c	1	2	3	4	5	6	7	8	9	10	11	12
S	1	1										
1	1											
2	1	1										
3	1	1	1									
4	1	2	1	1								
5	1	2	2	1	1							
6	1	3	3	2	1	1						
7	1	3	4	3	2	1	1					
8	1	4	5	5	3	2	1	1				
9	1	4	6	6	5	3	2	1	1			
10	1	5	8	9	7	5	3	2	1	1		
11	1	5	10	11	10	7	5	3	2	1	1	
12	1	6	13	15	13	10	7	5	3	2	1	1

Figure 6. The triangle matrix for the number of SS states at $S = 1\text{--}12$. Explanations are given in the text.

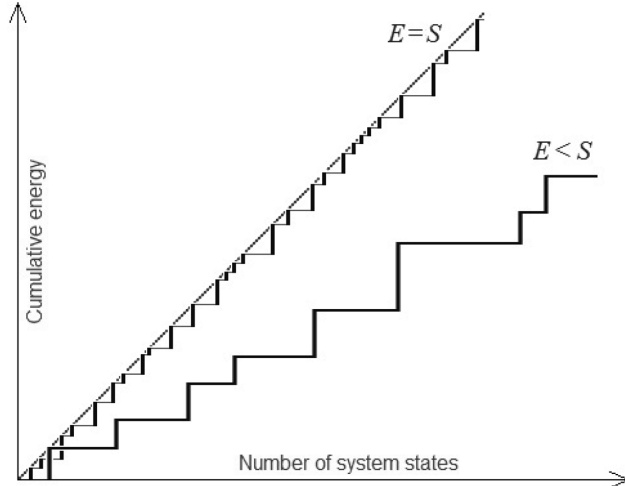


Figure 7. A schematic illustration of the step-like behaviour of cumulative energy E versus the number of states S for two cases of seismicity in the SS. The occurrence of weak seismicity (light line) is frequent and close to the equilibrium line, where $E = S$. Instances of moderate-strength seismicity (solid black line) are relatively rare and farther away from equilibrium, with $E < S$.

equilibrium, respectively. The first condition implies that the system stays homogeneous in the equilibrium state, while for $E < S$, indicator earthquakes transform the non-equilibrium system into a seismically inhomogeneous state. Whether earthquake occurrences are frequent or rare depends on a system's trajectory and its time steps. If in all steps of time without skipping indicator earthquakes take place, then earthquakes occur frequently; otherwise, they are rare.

Using (11), we construct a triangle matrix of seismic state probabilities p_i (Table 1). In this table, columns n on the right-hand side show the total number of possible trajectories, the probability value $\tilde{p} = 1/S$ without degeneracy, the mean of cumulative energy $\langle E \rangle$ calculated using (12), and the cumulative energy value \hat{E} at the maximum likelihood p_{\max} . It is apparent that there is only a small discrepancy between $\langle E \rangle$ and \hat{E} .

Fig. 8 shows the probability distribution plot of the SS with energy E_{ci} at fixed $S = 1\text{--}12, 20$. The probability distribution is an asymmetric function of E . As S increases, the energy value \hat{E} at maximum probability shifts farther to the right at a decreasing rate. Therefore, the highest possible $E = S$ energy states are extremely rare at large S . Thus, for $S = 4\text{--}23$, the most probable state is $\hat{E} = 2\text{--}6$. In addition, there is the following pattern: $\hat{E} = 2$ for two states $S = 4, 5$; $\hat{E} = 3$ for three states $S = 6\text{--}8$; $\hat{E} = 4$ for four states $S = 9\text{--}12$; $\hat{E} = 5$ for five states $S = 13\text{--}17$; $\hat{E} = 6$ for six states $S = 18\text{--}23$. We can write a recurrent relation

$$S_{\hat{E}} = S_{\hat{E}-1} + \hat{E}, \quad (15)$$

which at $\hat{E} = 7$ gives $S_7 = 23 + 7 = 30$, and so on. The recurrence relation (15) can be written as

$$S_{\hat{E}} = \sum_{n=1}^{\hat{E}} n + 2, \quad \hat{E} = 1, 2, 3, \dots, \quad (16)$$

where the number 2 appears because the first three states of SS in Fig. 4 are not degenerate. This implies that the discrete number of SS states $S_{\hat{E}}$ is defined by the sum of a natural series of cumulative energy values. The discrete set of numbers, $S_{\hat{E}} = 3, 5, 8, 12, 17, 23, 30, 38, 47, 57, 68, \dots$, differs by a factor of 2 from the known ‘magic’ numbers of Pascal’s triangle (Conway & Guy 1996). Eq. (16) provides exact calculation of step functions for an ideal homogeneous SS at arbitrary S (Fig. 9). At larger S values, an approximated dependence between \hat{E} and S parameters can be interpolated using the power-law relationship

$$E = \beta S^a, \quad (17)$$

where $0 < a < 1$. Fig. 9 illustrates a simple case where $\beta = 1$ and $E = S^a$. The best fit value $a = 0.58$ is calculated on the basis of discrete \hat{E}_i values and recurrent eq. (15) with $a = 1/97 \sum_{i=4}^{100} \log \hat{E}_i / \log S_i$.

The found probability distribution seen in Fig. 8 is close to the Poisson distribution, $P(x, \lambda) = \frac{1}{x!} \lambda^x e^{-\lambda}$ (Rade & Westergren 2004) with two parameters (x, λ). Here, $x = 1, 2, 3, \dots$ is the actual number of occurrences of an event, and λ is the expected number of occurrences during the given interval. Replacing $x = E$ and $\lambda = \hat{E}$, the Poisson function for an SS is reduced to

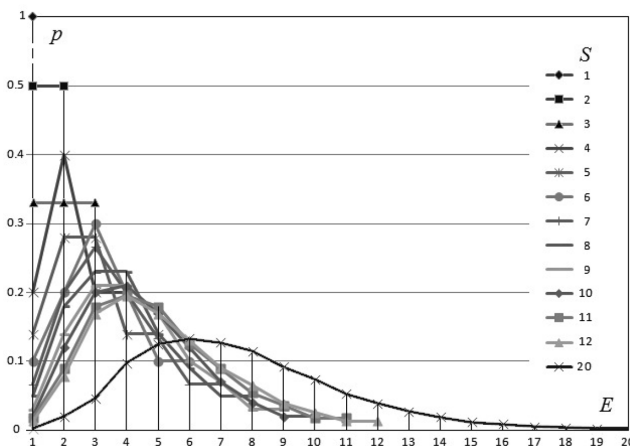
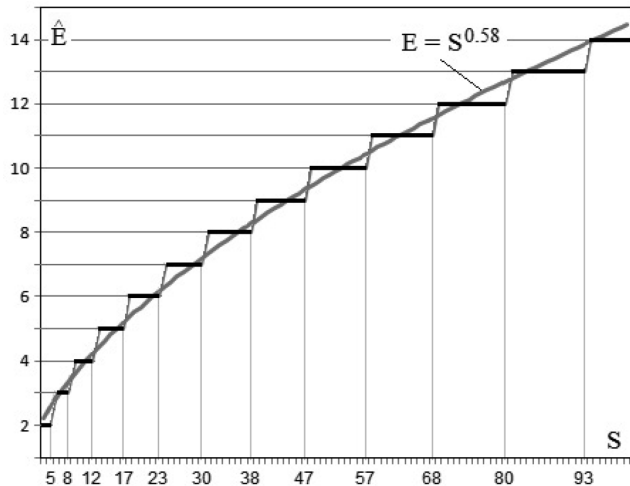
$$p(E) = \frac{1}{E!} (\hat{E})^E e^{-\hat{E}}. \quad (18)$$

Using this formula and recurrent relation (15), we can approximately calculate the probability distribution for any limited interval $E \in [1, S]$.

Eq. (17) for large S can be interpreted as follows. The seismic state of the initially ideal homogeneous SS tends, over time, to reach the maximal probable cumulative energy state E defined by the power law (17). In an ideal system, such behaviour is an intrinsic property of new cumulative parameter. It can also exist in a more complex, real SS with seismic inhomogeneities. Importantly, the instrumental observation periods for real SS are very short compared to their time evolution over hundreds of thousands or even millions of years. During this lengthly evolution, the SS inherit their primary fixed and acquired heterogeneities (Shaw 2004; Hillers *et al.* 2007). Constants a and β of the power law (17) describe the dynamics of non-equilibrium processes within cycles that lead to seismic inhomogeneities. In real SS, unlike ideal systems, there is noise. Data in earthquake catalogues also has limitations due to the variables such as sensitivity of seismic instruments (Kagan 2003). Therefore, when considering real systems, it is necessary to integrate elementary (action) parameter h_s (8), in accordance with the

Table 1. Pascal's triangle for probability states of system at $S = 1-12$. Explanations are given in the text.

E	1	2	3	4	5	6	7	8	9	10	11	12	n	\tilde{p}	$\langle E \rangle$	\hat{E}
S																
1	1.00												1	1.00	1.00	—
2	0.50	0.50											2	0.50	1.50	—
3	0.33	0.33	0.33										3	0.33	1.98	—
4	0.20	0.40	0.20	0.20									5	0.25	2.40	2
5	0.14	0.28	0.28	0.14	0.14								7	0.20	2.80	2 or 3
6	0.10	0.20	0.30	0.20	0.10	0.10							11	0.17	3.30	3
7	0.07	0.20	0.27	0.20	0.13	0.07	0.07						15	0.14	3.64	3
8	0.05	0.18	0.23	0.23	0.14	0.09	0.05	0.05					22	0.13	4.01	3 or 4
9	0.03	0.14	0.21	0.21	0.17	0.10	0.07	0.03	0.03				29	0.11	4.32	4
10	0.02	0.12	0.20	0.21	0.17	0.12	0.07	0.04	0.02	0.02			42	0.10	4.80	4
11	0.02	0.09	0.18	0.20	0.18	0.13	0.09	0.05	0.04	0.02	0.02		56	0.09	4.92	4
12	0.01	0.08	0.17	0.20	0.17	0.13	0.09	0.07	0.04	0.03	0.01	0.01	77	0.08	5.15	4

**Figure 8.** The calculated distribution of cumulative energy probabilities for detecting the system states where $S = 1-12, 20$.**Figure 9.** An illustration of the step function of discrete energies \hat{E} (maximum likelihood) at specific S values, computed for $S \in [4, 100]$.

weakest seismic microearthquake energy. For example, if catalogue completeness data begins with magnitude $M = 3.0$ (according to (1) $E = 10^{9.3} \text{ J}$), then an action parameter can be chosen that is much larger than h_s , that is, $\hbar_s = 10^{9.3} h_s$. Thus, real SS inhomogeneities are apparently uniform on a larger scale, once we redefine h_s by enlarging the \hbar_s parameter.

In general, constants a and β in power law (17) depend on dynamic characteristics of a system's geological structure. They may also vary significantly across seismic cycles that occur within the same system. Our goal is to determine the SS volume responsible for all seismic cycles that culminate in strong earthquakes and to find the set of E and S parameters that satisfy the power-law relationship (17) for given a and β constants. One must bear in mind that the time memory information hidden in $E(t)$ and $S(t)$ already emerges in (17), that is, in the fundamental relationship $E = E(S)$. In the next section, we find that, when this condition is imposed on a population of strong earthquakes in equilibrium, they form an ensemble within a uniquely defined SS.

4 TRAJECTORY DIAGRAM OF SS

4.1 Ensemble of strong earthquakes

The methods of fracture in mechanics of rocks have been adapted to describe faulting in the source of strong earthquakes (Anderson & Whitcomb 1973; Mjachkin *et al.* 1975; Scholz 1990; Sobolev & Ponomarev 2003). These models of earthquake sources were developed based on a comparison of laboratory data with the observed earthquake precursors. Such approach to the problem of earthquake preparation can describe only the local space domain of the SS. Moreover, the media parameters outside of the strong earthquake source can control the seismic energy radiation (Kostrov 1974; Rice 1980; Akopian 1995a). In contrast to traditional approaches we consider larger volumes of geological medium responsible for preparation of the ensemble of strong earthquakes. Definition of SS for a given seismically active region is also conceptually different from the arbitrary selected critical space-time domain used to identify precursors for the origin of specific seismic instability (main shock), given in advance by its location and magnitude (Dobrovolsky *et al.* 1979; Bowman *et al.* 1998; De Santis *et al.* 2010). In contrast, the location and magnitude of the predicted strong earthquake within SS are not known in advance. In addition, the set of indicator earthquakes are carrying information about both, the state of the media at any time and past history of strong earthquakes in the region. Therefore, any local model of a single earthquake source loses information about the interaction of different fault structures, collectively involved in a uniform seismotectonic process. The volume of geological medium within the configurations of SS on the surface and depth, being a complex tectonic formation, reacts to the external stress, periodically deviates from the state of equilibrium and restores a new state of equilibrium. In such an open system,

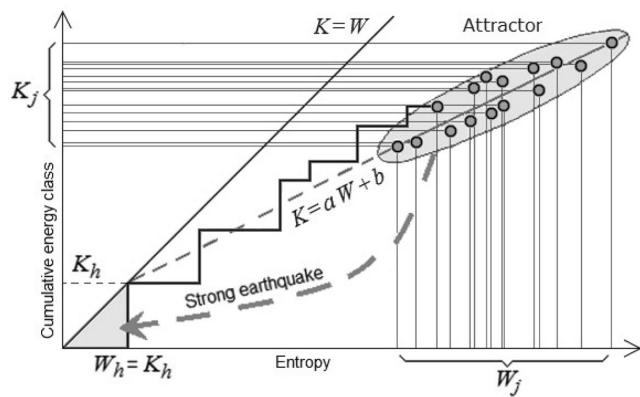


Figure 10. The attractor for an ensemble of strong earthquakes is in the form of an elliptical ‘cloud’ stretched along a straight line. The diagonal $K = W$ corresponds to a stable equilibrium state. K_h is determined by the threshold energy class for estimating significant drift of the SS from equilibrium (the intersection of the attractor line with diagonal). The trajectory starts from the region of equilibrium near the origin (triangular shaded area) and over a long time period falls into the attractor (elliptical shaded area) with critical points, indicating strong earthquakes. After each cycle the system returns to the origin to begin a new cycle (dotted arrow).

the total radiated energy of indicator earthquakes is not enough to restore balance until a strong earthquake occurs. Faulting and loss of continuity within the local area of strong earthquake sources is actually a process of returning the energy balance to equilibrium and restoring the seismic continuity (homogeneity) of the entire system.

The concept of an attractor is applied to the subset of critical points $\{E_j, S_j\}$ of strong earthquakes, occurring at different times t_j , for a given geological medium that attracts almost all trajectories. Fig. 10 shows an attractor on a trajectory diagram in the form of an elongated elliptical ‘cloud’. The cloud consists of well-defined SS that is created when strong earthquakes cooperate and form an ensemble. Scattered (‘cloud’) points $\{W_j, K_j\}$ of the ensemble occupy limited intervals along the axes, $W_{\min} \leq W_j \leq W_{\max}$ and $K_{\min} \leq K_j \leq K_{\max}$. We assume that, at the beginning of the seismic cycle, the SS, in the absence of sensitive seismic activity ($E \leq E_h$), is in equilibrium (at noise level) close to the origin (Fig. 10). Each trajectory of seismic cycles starts from the region of equilibrium near the origin (the triangular shaded area). Over a long time scale, a trajectory approaches the attractor region and terminates as a strong earthquake at some critical point. After the strong earthquake and subsequent aftershocks, the system returns to the origin (dotted arrow on Fig. 10), establishing a new equilibrium state. The evolution of the system involves multiple repetitions of such cycles. The required minimum energy for a random indicator earthquake to start a new trajectory is discussed in Section 4.2.

In fact, aftershocks, which are attenuation activity resulting from the last major earthquake, can be ignored in the preparation for the next strong earthquake. Since each strong earthquake in an ensemble (including its aftershocks) transforms the attractor into an area of equilibrium, one can consider the attractor to be a state of SS in dynamic equilibrium. In future articles, we will look at the effect of complex transformation processes on seismic equilibrium.

Here, we focus on long time scale earthquake preparation. Consider N seismic cycles (equal to the number of strong earthquakes with $M \geq M_{\text{th}}$) at the current stage of evolution, separated by times t_1, t_2, \dots, t_N . Each cycle is characterized by a corresponding seismic state S_1, S_2, \dots, S_N and cumulative energy E_1, E_2, \dots, E_N . Instead

of considering seismic cycles as system states at different times t_j , we can formally introduce N subsystems (seismic ensemble) that end in N different macroscopic states S_j . If all N seismic cycles are independent, then the total entropy of SS, consisting of all the formal subsystems in states S_j , is equal to the sum of the individual entropies W_j of the subsystems:

$$W(S) = \sum_{j=1}^N W(S_j), \quad \text{where } S = \prod_{j=1}^N S_j \quad (19)$$

provided $S_j < S_{\max}$; that is, SS entropy is an additive quantity of subsystem entropies. At the macroscopic level these functions satisfy the differential equation (Nicolis 1986):

$$S \frac{d^2 W}{dS^2} + \frac{dW}{dS} = 0. \quad (20)$$

The common solution of eq. (20) has the form

$$\tilde{W} = c_1 \log S + c_2, \quad (21)$$

where c_1 and c_2 are arbitrary constants.

As time increases, seismic cycle trajectories tend to reflect the power law. By taking the logarithm of (17), a simple relation can be established between entropy W and cumulative energy class $K = \log E$:

$$K = aW + b, \quad \text{at } W \geq W_{\min}, \quad \text{where } b = \log \beta \quad (22)$$

If eq. (22) is satisfied during all seismic cycles for the same constants a and b , we say that the SS, that is, discrete volume of lithosphere, is found. Thus, we assume that all strong earthquakes of the SS form an ensemble with constant parameters a, b , as they occur near the critical line (22). So, critical behaviour in an ensemble of strong earthquakes in the range $W_{\min} \leq W_j \leq W_{\max}$ occurs close to (22), where K_j and W_j are corresponding critical cumulative energy classes and entropies, respectively, for formal subsystem j . From entropy (21) of formal SS, constants c_1 and c_2 are derived for a particular solution \tilde{K} from common \tilde{W} satisfying eqs (20) and (22):

$$c_1 = a, \quad c_2 = b, \quad \tilde{W} = \tilde{K} = a \sum_{j=1}^N W(S_j) + b. \quad (23)$$

Conditions (23) means that the seismic cycles of an ensemble of strong earthquakes are independent. It means that, after every strong earthquake of an ensemble, the system (with some degree of certainty) comes into equilibrium and restores a seismically homogeneous state (continuity). In the next subsection, we show how to compute coefficients a and b for an ensemble of strong earthquakes in real systems.

This result demonstrates that the fundamental relationship (17) obtained between information entropy and cumulative energy for dynamic processes far from equilibrium in indicator earthquakes within seismic cycles (via statistical mechanics) applies, in some circumstances, to population ensembles of strong earthquakes in equilibrium.

4.2 Critical behaviour and attractor for real systems

Critical behaviour (22) in an ensemble of strong earthquakes for SS Sakhalin, Armenian Upland, Italy and Central California has previously been studied empirically (INTAS final report 1997; Akopian 1998a,b). These studies show that strong earthquakes form a set of critical points (attractor) in the shape of an ellipse near the critical line (22). Here we examine explanatory data used to test the

observed pattern. In practice, to find eq. (22), we need to solve the inverse regression problem. The catalogue provides empirical data for calculations of set of W_j and K_j parameters for N ended seismic cycles, that is, $\{W_j, K_j\}, j = 1, 2, \dots, N$. From these data measurements, average \bar{K} and \bar{W} are obtained (Rade & Westergren 2004):

$$\bar{K} = (1/N) \sum_{j=1}^N K_j, \quad \bar{W} = (1/N) \sum_{j=1}^N W_j, \quad (24)$$

the standard deviations σ_k and σ_w of two variables are

$$\sigma_w^2 = (1/N) \sum_{j=1}^N (W_j - \bar{W})^2, \quad \sigma_k^2 = (1/N) \sum_{j=1}^N (K_j - \bar{K})^2 \quad (25)$$

and their correlation parameter r is derived

$$r = \frac{\bar{W}\bar{K} - \bar{W}\bar{K}}{\sigma_w \sigma_k}. \quad (26)$$

This parameter measures the strength and direction of the linear relationship between W and K . The amount of deflection from a straight line reflects the degree of heterogeneity of the SS. The closer the value of coefficient r is to 1, the better the experimental data can be described by a linear equation. The least-squares regression (straight) line is given by

$$K_j^* = aW_j + b, \quad (27)$$

which minimizes the sum of squares of vertical distances from the line for observed scatter points. Here, star in eq. (27) emphasizes that this line provides a predicted response K^* for any W . Thus, the regression line defines a slope $a = r\sigma_k/\sigma_w$ and intercept $b = \bar{K} - a\bar{W}$. W_j are accurate statistical entropy values, while actual K_j values deviate from calculated values of K_j^* , $\varepsilon_j = |K_j^* - K_j|$. These deviations contain two components, $\varepsilon_j = \varepsilon'_j + \varepsilon''_j$. The stable parameter ε'_j reflects seismotectonic features of the SS (the degree and geometry of its fragmentation), while ε''_j describes random statistical errors and poor determination of the SS. For a well-defined SS, errors ε''_j can be minimized, $\varepsilon_j \approx \varepsilon'_j$. When there is an increase in the number of seismic cycles, the attractor may form steady

scattered points around the straight line (27). The deviation from averaged eq. (27) measures the estimated relative error of correlation ε :

$$\varepsilon = (1/N) \sum_{j=1}^N |K_j - \bar{K}| / K_j. \quad (28)$$

Overall, we studied more than 100 representative ensembles of strong earthquakes in different seismically active regions worldwide, with threshold magnitudes between $5.5 \leq M_{\text{th}} \leq 8.4$. Parameters a, b in eq. (27) for these ensembles of earthquakes varied in the range: $0.35 < a < 0.82$, $3 < b < 11.5$. As a rule, parameter b increases with an increase in the threshold magnitude. Thus, we can use catalogue data to plot a straight line that corresponds to the best fit regression line for power-law relationship (17) between W and K for given a, b . Calculated a, b, ε, r and other seismic parameters for 17 SS with different threshold magnitudes M_{th} , number of ended seismic cycles N are given in Table 2.

To calculate the parameters in Table 2 it is necessary to select the initial configuration and depth by compiling regional catalog for each SS. The selection of the initial SS boundaries and threshold magnitude of earthquakes requires knowledge on the region seismotectonics. To find accurate (final) configuration and depth of the SS (hence, the earthquake catalogue for SS) one needs to get solution of a direct and inverse regression problems through the variation of the system boundary and corresponding threshold magnitude (Akopian 1998a) using relationship (17) and criteria for the best fit to eqs (22)–(23). Thus, accurate determination of the SS is a rather complex problem based on the trial-and-error analysis.

The SS data in Table 2 are organized in descending order of threshold magnitude, M_{th} . Parameter T in Table 2 is a historical period of description of seismic processes in SS (in years) with the start date t_0 and the end date of the 2012. Therefore, a start date for each SS catalogue can be found, $t_0 = 2012 - T$. The choice of T is carried out based on reliable information about historical earthquakes of pre-instrumental period (before 1900). Such information is available for Armenian Upland, the catalogue ‘Caucasus’ (INTAS final report 1997), for the regions California, Italy and Tibet, see, for example, Ellsworth (1990), Camassi (2004) and Bilham (2004).

Table 2. Calculated parameters of the attractor for 17 seismic systems arranged in descending order of threshold magnitude M_{th} . T is the description time of seismic processes (in years) ending in 2012; L_m is the system maximum length (in km); N is the number of ended seismic cycles; a, b are parameters of linear regression (eq. 27) M_h is the minimal magnitude of a significant indicator earthquake; M_{max} is the maximal magnitude in the ensemble of strong earthquakes; ε is the correlation error percentage and r is the correlation coefficient.

Seismic system	M_{th}	T	L_m	N	a	b	M_h	M_{max}	ε per cent	r
Mega Japan (MJ)	8.4	116	1700	3	0.317	11.121	7.5	9.1	0.8	1.00
Mega Chile (MC)	8.3	106	3000	5	0.485	7.802	6.5	9.1	2.2	0.99
Tibet (Ti)	7.8	179	2750	6	0.465	8.172	6.6	8.6	1.7	0.98
Kamchatka (Ka)	7.8	112	1050	6	0.460	8.071	6.3	8.5	1.2	0.91
Hokkaido (Ho)	7.8	112	790	10	0.470	8.113	6.6	8.4	1.6	0.91
Japan (J)	7.8	106	1700	14	0.644	4.952	5.5	8.4	1.5	0.94
Taiwan (Ta)	7.7	111	500	6	0.489	7.450	5.9	8.1	0.9	0.91
Eastern Turkey (ET)	7.2	182	1000	6	0.455	7.496	5.4	7.9	0.8	0.97
Central Kuril (CK)	7.0	96	330	6	0.436	8.160	5.8	7.9	1.9	0.98
Armenian Upland (AU)	6.6	182	1000	16	0.565	5.540	4.9	7.5	2.7	0.82
Italy (It)	6.2	158	1280	19	0.500	6.680	5.2	7.3	2.1	0.93
NE Iran (Ir)	6.2	108	930	7	0.498	6.528	5.0	7.3	2.1	0.97
Sakhalin (Sa)	6.2	106	990	5	0.580	4.937	4.3	7.5	2.6	0.99
Central California (CC)	6.0	147	350	18	0.486	6.598	4.9	7.0	2.2	0.88
Western Caucasus (WC)	6.0	107	600	5	0.501	5.887	4.3	6.8	2.6	0.99
Los Angeles (LA)	5.8	110	260	4	0.562	5.002	4.1	6.6	1.0	0.91
Parkfield (P)	5.5	132	60	5	0.595	4.189	3.5	6.2	0.8	0.98

The completeness and reliability of information about strong and indicator earthquakes at data processing differs at various time intervals. For this reason, the priority was given to earthquakes in the instrumental period. Almost for all systems shown in Table 2 is possible to compile an uniform representative catalogue with $M \geq M_h$ for an entire instrumental period, since the lower threshold of indicator earthquakes in most catalogues begins with $M_h \geq 4.0$. Uneven representation of weak seismicity in catalogues in time periods from 1900 to 1973 and from 1973 to 2012 does not significantly affect the results for the SS with low values of M_h because of the small contribution to cumulative energy (Appendix A).

Here, we explain in detail the choice of threshold M_{th} and maximum M_{max} magnitudes for the SSs listed in Table 2. These values show the conditional lower and upper limits for the magnitudes ($M_{th} \leq M < M_{max}$) of ensembles of strong earthquakes in the SS, well described by regression eq. (27). At construction of attractors for real SS we used a hierarchical approach where the system is divided into the subsystems and threshold magnitude is decreased. At such approach, some indicator earthquakes of the SS are considered strong in a subsystem, and they form an ensemble with a lower energy level in the range $M_{th}^1 \leq M < M_{max}^1$, where $M_{th}^1 < M_{th}$ and $M_{max}^1 < M_{max}$. Thus, in Table 2, SS Japan is a subsystem of SS Mega Japan, SS Armenian Upland is a subsystem of the SS Eastern Turkey, and SS Parkfield is a subsystem of the SS Central California. As one can see (Appendix B), the sizes of the first two subsystems coincide with the sizes of corresponding systems, while a size of subsystem Parkfield is much smaller than the size of SS Central California. The threshold magnitudes of all subsystems are less than threshold magnitudes of corresponding systems.

In SS Mega Japan, since 1896 there were three catastrophic earthquakes: Sanriku 1933, $M = 8.6$; Nankaido 1946, $M = 8.4$; and Tohoku 2011, $M = 9.0$ according to the NOAA/USGS catalogue (see also <http://www.ngdc.noaa.gov/nndc/struts/form?t=101650&s=1&d=1>) form an ensemble in magnitude range $8.4 \leq M < 9.1$. In the SS Japan, the instability points of the three strongest earthquakes deviate significantly from the regression line, while others in the range $7.8 \leq M < 8.4$ are well described by eq. (27) and form an ensemble in the subsystem. When the points of instability of the strongest earthquakes are located significantly above the attractor, there might be a deficit in entropy production (Akopian 1998a). Usually this occurs when there are mega earthquake in the system. One can use a larger SS and/or larger threshold magnitude for a better description in such cases. Since earthquake magnitudes are discrete, there is usually a gap between the lowest-magnitude of strong earthquakes and the highest-magnitude of indicator earthquake, between the maximum magnitude in ensemble and the strongest earthquake. Therefore, the choice of lower and upper threshold M_{th} and M_{max} magnitudes becomes conditional, uncertain within this gap. However, over time, with increasing statistics available regarding seismic cycles, these threshold values can also be specified and corrected. The details on SS Mega Japan, Japan and Eastern Turkey, based on trajectory and energy diagrams and the results of monitoring of recent destructive earthquakes Tohoku (2011 March 11) and Van (2011 October 23) will be given in Akopian (2013) and Akopian & Rogozhin (2013).

Cases of close grouping of earthquakes near threshold magnitude are sometimes observed. If one of them has a magnitude somewhat less than the threshold value, this earthquake should be considered as an indicator, and the whole SS is not yet responsible for its preparation. Such a problem arose when we tried to study the earthquakes sequence in the Parkfield segment of SAF as a result of a selective reaction of the Central California and Parkfield systems to signif-

icant earthquakes (Appendix B). This indicates that the study of earthquakes with magnitudes close to threshold values is worthy of special attention.

A detailed description and calculation of the parameters for relatively simple SS Sakhalin is given in Appendix A. The configuration, depth, epicentres of indicator earthquakes, and zones of instability (source zones of strong earthquakes) on the map for the systems, listed in Table 2 and also are given in Appendix B. You can see that over time zones of the instability of strong earthquakes tend to fill the significant heterogeneity of the system. The ensembles with more completed cycles provide more accuracy that can be used to determine the zones of instability distribution and ultimately the seismic attractor. Based on the trajectory diagram, one can monitor the dynamics and critical behaviour of the SS to forecast strong earthquakes in time and space (Appendix A). Depending on how the path is approaching the attractor, we can predict different manifestations of seismicity before a strong earthquake, such as swarms, calms, triggers, foreshocks and aftershocks (Akopian 1998a; Akopian & Popov 2010). The calculated values for the correlation error ε and the correlation coefficient r vary in the range $0.8 \leq \varepsilon \leq 2.7$ per cent and $0.82 \leq r \leq 1$. This means that, within an attractor of real SS, the quantities W_j, K_j are strongly correlated with statistical functional dependence (27). Table 2 shows that, for the well-defined SS of Armenian Upland, Central California, Italy and Japan, with a large number of seismic cycles, the correlation coefficients are low: 0.82, 0.88, 0.93 and 0.94. This is a measure of the fragmentation and multidirectional fault structure of SS that generate strong earthquakes. The correlation coefficient for Armenian Upland shows that fragmentation here is high (Akopian 1998b), while it is less for Japan.

At the beginning of a seismic cycle, indicator earthquakes occur randomly. Over time, they start to compete and correlate with one another. We can define the minimum significant energy level (magnitude) of an indicator earthquake that starts a new trajectory. The upper energy level in the initial seismically homogeneous condition (equilibrium) can be estimated by extrapolating eq. (27) up to the intersection with diagonal line ($K = W$) for stability (Fig. 10):

$$K_h = b/(1 - a). \quad (29)$$

We assume that, below this value, trajectories are close to the state equilibrium (Fig. 10). The deviation of the trajectory from the equilibrium state for an ensemble of earthquakes in the SS becomes significant when the indicator earthquake energy is larger than $E \geq 10^{K_h}$. Using (29), we can find the required minimum energy for an indicator earthquake that marks the start of the next cycle (trajectory) of strong earthquakes:

$$E_h = 10^{b/(1-a)}. \quad (30)$$

By using (1), we also find the minimal magnitude of such an indicator earthquake M_h . Thus, a new cycle of seismic activity, when calculating trajectories, starts with an indicator earthquake with $M \geq M_h$, which can be determined once sensitive aftershocks from the last strong earthquake are removed. For reliable calculation of magnitude, M_h is considered to be greater than the smallest magnitude M_{min} of all representative earthquakes in the existing catalogue of the SS region ($M_{min} \leq M_h < M_{th}$). Table 2 shows calculated threshold M_h values and maximum magnitudes in ensembles of strong earthquakes for the 17 systems. Fig. 11 illustrates M_h and maximal value M_{max} (magnitude) in an ensemble of strong earthquakes for the same SS regions, arranged in descending order by threshold magnitudes. Thus, each seismic ensemble can be characterized by a minimum (lower bound) threshold M_h for a representative

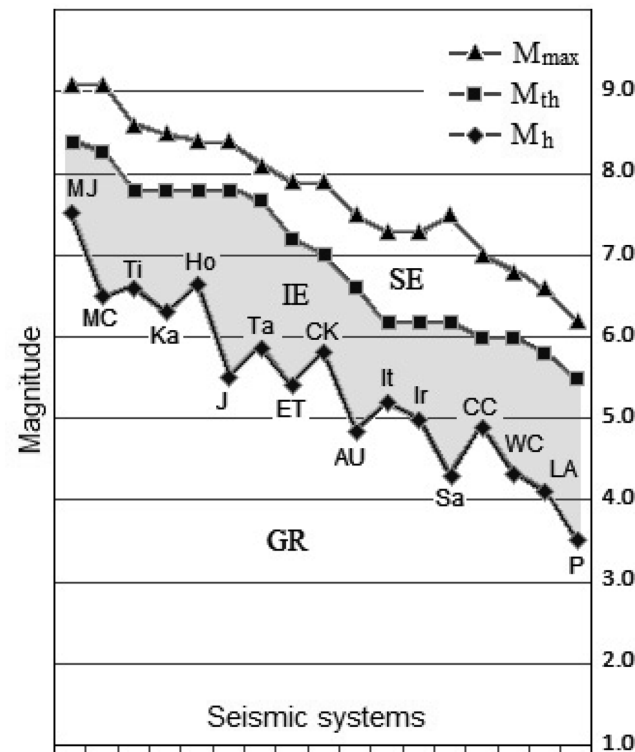


Figure 11. The graph shows the thresholds M_h and M_{\max} for different SS in Table 2 arranged in descending order by M_{th} . GR denotes the magnitude range where the Gutenberg–Richter law is valid, IE determines the range (shaded) of random indicator earthquakes, and SE corresponds to strong earthquake magnitudes. Abbreviations of SS names are the same as in Table 2.

indicator earthquake, as well as by a maximum (upper bound) threshold magnitude M_{th} . The main energy contribution to the trajectory of strong earthquake preparation comes from the input of indicator earthquakes in the range $M_h \leq M \leq M_{\text{th}}$, where the GR law (calculated in accordance with the parameters for various SS) is usually violated. Here (and in Fig. 11), we mean the GR law as calculated in seismic cycles for the SS volume with minimum step $\Delta M = 0.2$ in magnitude. The GR law is well established in the range $M < M_h$, where there is a large number of weak earthquakes, but their contribution to cumulative energy is still negligible (despite frequent occurrences). As it happens, the mean square root error in determining the slope of the frequency is inversely proportional to the square root of the number of applied earthquakes. The violation of the GR law at $M \geq M_h$ is due to a reduction in the number of earthquakes in the seismic cycle and to an increase in the (standard) error seen in the slope of the frequency. More details on this issue are presented regarding the number of seismic cycles in SS Sakhalin (Appendix A). The minimum threshold energy E_h of the system divides SS states into microscopic and macroscopic ones. In general, indicator earthquakes at the microscopic level improve the accuracy of calculations and can be included for short-term forecasting.

5 CONCLUSION

The real-time evolution and critical behaviour of seismogenic media responsible for the preparation of strong earthquakes are examined using statistical probability in terms of information entropy, which puts cumulative energy and entropy quantities on an equal footing. The critical behaviour of the SS is described by the revealed

power-law relationship between these two parameters. Clustering of earthquakes near critical points (attractor) in an ensemble of strong earthquakes reflects the dynamics of heterogeneous behaviour of a specific (lithosphere) volume to the external compression. Statistical computation for multiple seismic cycles in a real SS shows a strong correlation with power-law seismic instabilities for non-equilibrium indicator earthquake states. The trajectory diagrams describe the dynamics and critical behaviour of the SS, and can be used to monitor and forecast earthquakes at long, middle and short stages of preparation. They also describe various manifestations of seismic activity that occur before the formation of significant seismic inhomogeneity. We also present inverse methods and results of quantitative calculations of attractors for real SS with different configurations, depending on the plate-tectonic situation. Introduction of the concept of SS provides distinct lower and upper threshold values which allow quantify earthquakes on strong, indicators and weak magnitudes depending on the scale of the seismotectonic structures. We attempt to understand the evolution of geological media and provide a new, comprehensive perspective for known seismic phenomena. Work is currently in progress to refine details about seismic processes, such as structures that form an ensemble of strong earthquakes, dissipative processes, and the reestablishment of energy balance by restoring equilibrium.

ACKNOWLEDGEMENTS

The authors would like to acknowledge G.A. Sobolev for useful discussions and A. De Santis and L. Alviti for a careful reading of the manuscript and valuable comments to improve the paper. We would also like to thank our anonymous reviewers for thoughtful and constructive comments.

REFERENCES

- Akopian, S.Ts., 1995a. Entropy of a seismic system and a new seismic law, *Dokl. Russ. Akad. Nauk*, **340**, 531–535.
- Akopian, S.Ts., 1995b. Seismic entropy monitoring and earthquake prediction problem, *Dokl. Russ. Akad. Nauk*, **341**, 247–250.
- Akopian, S.Ts., 1998a. Quantitative description of seismic processes based on seismic entropy, *Izv. Russ. Akad. Nauk, Fiz. Zemli*, **1**, 11–26.
- Akopian, S.Ts., 1998b. Description of seismic processes on the Armenian Upland based on seismic entropy, in *Papers Presented at XXVI General Assembly of the ESC*, Tel Aviv, Israel, August 23–28, pp. 150–154.
- Akopian, S.Ts., 2013. Seismic systems of the Japan, entropy and monitoring of the mega earthquake Tohoku on March 11, 2011, *Problems Eng. Seismol.*, **40**, in press.
- Akopian, S.Ts. & Popov, E.A., 2010. Monitoring induced seismicity based on seismic entropy method, *Abstracts, Induced Seismicity EC GS–FKPE Workshop*, 15–17 November, Luxembourg, pp. 3–4.
- Akopian, S.Ts. & Rogozhin, E.A., 2013. Modeling kinematics of the Tauro–Caucasus region and dynamics of strong earthquake preparation with $M \geq 7.1$. *Problems Eng. Seismol.*, **40**, 5–24, in press.
- Al-Kindy, F.H. & Main, I.G., 2003. Testing self-organized criticality in the crust using entropy: a regionalized study of the CMT global earthquake catalogue, *J. geophys. Res.*, **108**, 2521–2529.
- Anderson, D.L. & Whitcomb, J.H., 1973. The dilatancy-diffusion model of earthquake prediction, in *Proceedings of the Conference on Tectonic Problems of the San Andreas Fault System*, pp. 417–426, eds Kovach, R.L. & Nur, A., Stanford Univ. Press.
- Anderson, P.W., 1991. Is complexity physics? Is it science? What is it? *Phys. Today*, **44**, 9–11.
- Bak, P. & Tang, C., 1989. Earthquakes as a self-organized critical phenomenon, *J. geophys. Res.*, **94**, 15 635–15 637.

- Barriere, B. & Turcotte, D.L., 1994. Seismicity and self-organized criticality, *Phys. Rev. E*, **49**, 1151–1160.
- Bilham, R., 2004. Historical studies of earthquakes in India, *Ann. Geophys.*, **47**, 839–858.
- Bowman, D.D., Ouillon, G., Sammis, C.G., Sornette, A. & Sornette, D., 1998. An observational test of the critical earthquake concept, *J. geophys. Res.*, **103**, 24 359–24 372.
- Camassi, R., 2004. Catalogues of historical earthquakes in Italy, *Ann. Geophys.*, **47**, 645–657.
- Conway, J.H. & Guy, R.K., 1996. *The Book of Numbers*, Springer-Verlag, pp. 68–70.
- De Santis, A., Cianchini, G., Qamili, E. & Frepoli, A., 2010. The 2009 L'Aquila (Central Italy) seismic sequence as a chaotic process, *Tectonophysics*, **496**, 44–52.
- De Santis, A., Cianchini, G., Beranzoli, L., Favali, P. & Boschi, E., 2011. The Gutenberg-Richter law and entropy of earthquakes: two case studies in central Italy, *Bull. seism. Soc. Am.*, **101**, 1386–1395.
- Dewar, R., 2003. Information theory explanation of the fluctuation theorem, maximum entropy production and self-organized criticality in non-equilibrium stationary states, *J. Phys. A Math. Gen.*, **36**, 631–641.
- Dobrovolsky, I.P., Zubkov, S.I. & Miachkin, V.I., 1979. Estimation of the size of earthquake preparation zones, *Pageoph*, **117**, 1025–1044.
- Ellsworth, W.L., 1990. Earthquake history, 1769–1989, in *The San Andreas Fault System*, Chapter 6, pp. 153–181, ed. Wallace, R.E., US Geological Survey Professional Paper 1515.
- Field, E.H. et al., 2009. Uniform California Earthquake Rupture Forecast, Version 2 (UCERF 2), *Bull. seism. Soc. Am.*, **99**, 2053–2107.
- Geller, J.R., 1997. Earthquake prediction: a critical review, *Geophys. Res. Lett.*, **131**, 425–450.
- Gutenberg, B. & Richter, C.F., 1954. *Seismicity of the Earth and Associated Phenomena*, 2nd edn, Princeton University Press.
- Gutenberg, B. & Richter, C.F., 1956. Magnitude and energy of earthquakes, *Ann. Geofis.*, **9**, 1–15.
- Haken, H., 1978. *Synergetics*, Springer-Verlag.
- Hillers, G., Mai, P.M., Ben-Zion, Y. & Ampuero, J.-P., 2007. Statistical properties of seismicity of fault zones at different evolutionary stages, *Geophys. J. Int.*, **169**, 513–533.
- INTAS final report, 1997, *INTAS 94–0232 (Italy, France, Russia, Armenia). Short-term Dynamics of Seismicity: New Theoretical Base and Implications to Seismic Risk Reduction*, Coordinator Prof. L. Bertocchi, ICTP, Trieste, Italy.
- Jaynes, E.T., 1979. Where do we stand on maximum entropy? in *The Maximum Entropy Formalism*, pp. 15–118, eds Levine, R.D. & Tribus, M., M.I.T. Press.
- Johnson, L.R., 2010. An earthquake model with interacting asperities, *Geophys. J. Int.*, **182**, 1339–1373.
- Jordan, T.H. et al., 2011. Operational earthquake forecasting: state of knowledge and guidelines for utilization, *Ann. Geophys.*, **54**, 315–391.
- Kagan, Y.Y., 2000. Probabilistic forecasting of earthquakes, *Geophys. J. Int.*, **143**, 438–453.
- Kagan, Y.Y., 2003. Accuracy of modern global earthquake catalogs, *Phys. Earth planet. Inter.*, **135**, 173–209.
- Kanamori, H., 2004. The diversity of the physics of earthquakes, *Proc. Jpn. Acad.*, **B80**, 297–316.
- Kolmogorov, A.N., Jurbenko, I.G. & Prochorov, A.V., 1982. *Vvedenie v teoriu veroyatnostey (Introduction to Probability Theory)*, Bibliotekha "Kvant", Nauka.
- Kostrov, B.N., 1974. Seismic moment, earthquakes energy and seismic flow of rock masses, *Izv. Akad. Nauk SSSR, Fiz. Zemli*, **1**, 13–21.
- Landau, L.D. & Lifshits, E.M., 1980. *Statistical Physics, Part 1, Vol. 5: Course of Theoretical Physics*, 3rd edn, Elsevier.
- Levin, B.W., Sasorova, E.V., Borisov, S.A. & Borisov, A.S., 2010. Estimating the parameters of small earthquakes and their signals, *Vulkanologiya i Seismologiya*, **3**, 60–70.
- Main, I.G. & Al-Kindy, F.H., 2002. Entropy, energy, and proximity to criticality in global earthquake populations, *Geophys. Res. Lett.*, **29**, doi:10.1029/2001GL014078.
- Main, I.G. & Naylor, M., 2010. Entropy production and self-organized (sub)criticality in earthquake dynamics, *Phil. Trans. R. Soc. A: Math., Phys. Eng. Sci.*, **368**, 131–144.
- Mjachkin, V.I., Brace, W.F., Sobolev, G.A. & Dicterich, J.H., 1975. Two models for earthquake forerunners, *Pure. appl. Geophys.*, **113**, 169–181.
- Mogi, K. & Mochizuki, H., 1983. Observation of high frequency seismic waves by a hydrophone directly above the focal region of the 1980 earthquake (M6.7) off the east coast of the Izu Peninsula, Japan, *Earthq. Predict. Res.*, **2**, 127–148.
- Molnar, P., Anderson, R.S. & Anderson, S.P., 2007. Tectonics, fracturing of rock, and erosion, *J. geophys. Res.*, **112**, F03014, doi:10.1029/2005JF000433.
- Nicolis, J., 1986. *Dynamics of Hierarchic Systems: An Evolutionary Approach*, Springer-Verlag.
- Nicolis, G. & Prigogine, I., 1989. *Exploring Complexity: An Introduction*, Freeman & Co.
- Pathria, R.K., 2005. *Statistical Mechanics*, 2nd edn, Elsevier.
- Poplavskaya, L.N. et al., 2006. *Regional Catalog of Sakhalin Earthquakes 1905–2005*, Russ. Akad. Nauk.
- Prigogine, I., 1980. *From Being to Becoming: Time and Complexity in the Physical Sciences*, Freeman & Co.
- Rade, L. & Westergren, B., 2004. *Mathematics Handbook for Science and Engineering*, 5th edn, Springer-Verlag.
- Rautian, T. & Leith, W., 2002. *Composite regional catalogs of earthquakes in the Former Soviet Union*, U.S. Geological Survey Open File Report 02–500, pp. 1–53.
- Rice, J., 1980. The mechanics of earthquake rupture, in *Physics of the Earth's Interior*, pp. 555–649, eds Dziewonski, A.M. & Boschi, E., North-Holland.
- Rivera, L. & Kanamori, H., 2002. Spatial heterogeneity of tectonic stress and friction in the crust, *Geophys. Res. Lett.*, **29**, doi:10.1029/2001GL013803.
- Rundle, J.B., Klein, W. & Tiampo, K.F., 2000. Linear pattern dynamics in nonlinear threshold systems, *Phys. Rev. E*, **61**, 2418–2431.
- Scholz, C.H., 1968. The frequency-magnitude relation of microfracturing in rock and its relation to earthquakes, *Bull. seism. Soc. Am.*, **58**, 399–415.
- Scholz, C.H., 2002. *The Mechanics of Earthquakes and Faulting*, 2nd edn, Cambridge Univ. Press.
- Shannon, C.E., 1948. A mathematical theory of communication, *Bell Syst. Tech. J.*, **27**, 379–423, 623–656.
- Shaw, B.E., 2004. Dynamic heterogeneities versus fixed heterogeneities in earthquake models, *Geophys. J. Int.*, **156**, 275–286.
- Sobolev, G.A. & Ponomarev, A.V., 2003. *Fizika zemletryasenij i predvestniki (Physics of Earthquakes and Precursors)*, Nauka.
- Solovev, S.L. (Ed.), 1977. *Seismic Zoning of Sakhalin (Seismicheskoe raionirovanie Sakhalina)*. Collection of articles, Akad. Nauk SSSR.
- Teng, T.L. & Heney, T.H., 1981. The detection of nanoearthquakes, in *Earthquake Prediction: An International Review*, Vol. 4, pp. 533–542, eds Simpson, D.W. & Richards, P.G., AGU, Maurice Ewing Series.
- Tsuboi, C., 1956. Earthquake energy, earthquake volume, aftershock area, and strength of the Earth's crust, *J. Phys. Earthq.*, **4**, 63–66.
- Tsuboi, C., 1965. Time rate of earthquake energy release in and near Japan, *Proc. Jpn. Acad.*, **41**, 392–397.

APPENDIX A: SEISMIC SYSTEM OF SAKHALIN

Here, some results presented in this article are illustrated using the simplest SS example, Sakhalin Island (Russia). Seismicity and the geological and geophysical characteristics of the sources of strong earthquakes in Sakhalin have been studied extensively (Solovev 1977). Some aspects of the SS Sakhalin have already been described in detail (Akopian 1998a). As this is published, there has been one strong earthquake (2000) and four completed seismic cycles since 1907. A new cycle started in 2000, and currently the system is in preparation for the next strong earthquake. Due to space limitations, we can only briefly describe SS Sakhalin here.

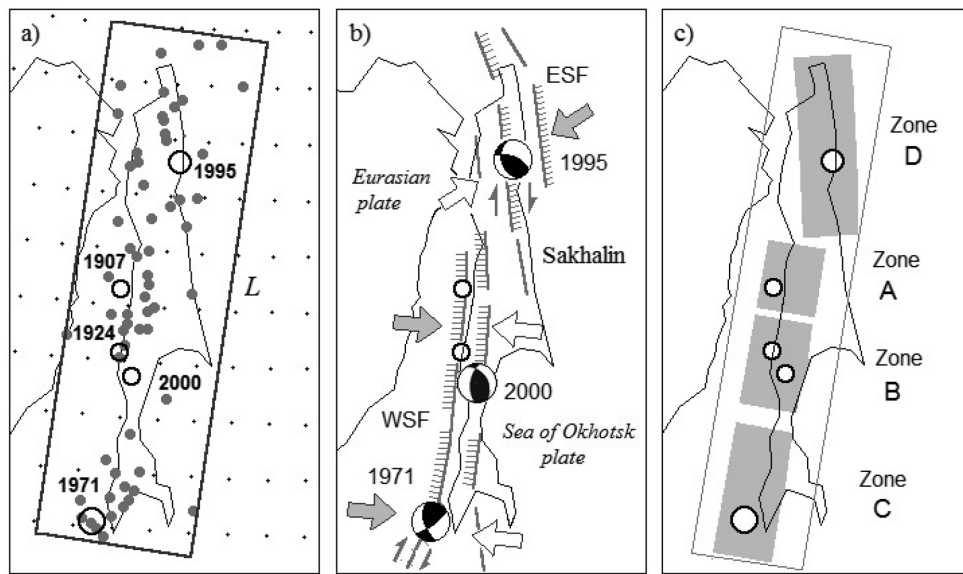


Figure A1. Sakhalin system details: (a) Indicator earthquakes with $M \geq 5.0$ (filled circles), and configuration L of SS Sakhalin; (b) Active faults and focal mechanisms of the Moneron, Neftegorsk and Ulegorsk earthquakes. ESF, WSF are the East and West Sakhalin faults. The directions of compressive stresses are indicated by arrows: black – the thrusting plate, light – the underthrusting plate; (c) Source zones of SS Sakhalin after five strong earthquakes. Open circles on the figures are the strong earthquake epicentres with $M > 6.2$.

and show the changes that occurred in the system from 1996 to 2012. Calculations were carried out on the basis of the earthquake catalogue for Sakhalin (Poplavskaya *et al.* 2006), with additional data from the USGS/NEIC catalogue (http://www.earthquake.usgs.gov/earthquakes/equarchives/epic/code_catalog.php). All calculations were performed on a scale of magnitude M_s . The distribution of the epicentres of shallow indicator earthquakes with magnitudes $M \geq 5.0$ for 1905–2012 allows a determination of configuration L on the surface (which includes Sakhalin Island and the shelf) and depth $H = 40$ km for the SS (Fig. A1a). The SS is found by the trial-and-error method by varying threshold magnitudes and bounds of the initially selected volume of the system chosen according to a plate-tectonic model of the region. SS Sakhalin is a good example because for configuration L , depth H and threshold magnitude $M_{th} = 6.2$, the relationship in eq. (22) is satisfied and has been empirically verified as per eq. (30) in Akopian (1998a):

$$K_c = 0.698 W + 2.891 \quad W > 15.70 \quad (\text{A1})$$

This regression equation was derived from calculated data K_{cj} and W_j ($j = 2–4$) for three seismic cycles of strong earthquakes (1924, 1971 and 1995, respectively). The system configuration includes two fault systems: the West Sakhalin Fault (WSF) in the southern/central parts of the system, and the East Sakhalin Fault (ESF) in the northern part, both of which are associated with the epicentres of strong earthquakes (see Fig. A1b). The Eurasian and Sea of Okhotsk plates, which interact in the Sakhalin area along these faults, control the complex tectonic processes associated with strong earthquakes in this region. Along its length of more than 1000 km, the system reaches a depth of 40 kilometres and includes the hypocentres of crustal indicator earthquakes. Table A1 shows data for all strong earthquakes on Sakhalin Island from 1906 to 2012. Cumulative parameters K_c and W for the seismic cycles are calculated using eqs (2), (3) and (5). In Table A1, we used energy class $K = 8.0 + 1.1 M$ at $M \geq 6.0$, and $K = 4.0 + 1.8 M$ at $M < 6.0$ (Rautian & Leith 2002). The minimum time step δt was set to 1 month. Fig. A1(c) indicates A, B, C and D zones of SS Sakhalin, which include the locations of all past strong earthquakes. These

areas determine forecast accuracy across space in SS Sakhalin after five seismic cycles. Using maps of active faults allows for the narrow prognostication of areas where strong earthquakes are expected in SS configuration L . The last strong earthquake (2000) occurred near the epicentre of the 1924 earthquake in zone B. Fig. A2 shows graphs of cumulative energy (2) and entropy (5) in the seismic cycles of SS Sakhalin (contributions of aftershocks are excluded). The average frequency of the three completed seismic cycles (without the current unfinished cycle) in SS Sakhalin since 1907 is 23 yr.

Fig. A3 shows the trajectory diagram of SS Sakhalin. Its linear zone of instability (seismic attractor), based on five critical points $\{W_j, K_{cj}\}, j = 1–5$, is well approximated by the regression line

$$K_c = 0.580 W + 4.914 \quad W > 15.70. \quad (\text{A2})$$

Since the earthquakes in Table A1 form an attractor, described by regression line (A2), they form an ensemble of strong earthquakes for SS Sakhalin. Extrapolation of this line to the intersection with the diagonal equilibrium line (Section 4.1) determines the minimum threshold of indicator earthquakes $K_h = 11.7$, $M_h = 4.3$ ($m_b = 4.9$). There is no direct one-to-one correspondence between body wave magnitude m_b and surface wave M_s . For SS Sakhalin, we use approximate relation $m_b = 2.3 + 0.60 M_s$. The seismicity level with $K < 11.7$ can be considered to be microscopic. The sources of these weak earthquakes across large areas are distributed relatively uniformly within SS Sakhalin. Weak earthquakes associated with lower-order tectonic heterogeneity (fracture) form background seismicity but only slightly affect the behaviour of the system as a whole in preparation for a strong earthquake. On the trajectory diagram for SS Sakhalin, the critical areas of the attractor in W and K parameter space (Fig. A3) correspond to A, B, C and D zones on the tectonic map (see Figs A1b and c). These areas have an average width ΔK_p and $\Delta W_p = 0.24$, which form instability areas that include the points of the attractors.

For practical forecasting, the assessment of these areas is important. Forecast accuracy over time depends on their size. The prognoses depend on the accuracy of the catalogues, the number of ended seismic cycles, the correlation coefficient, and so on.

Table A1. Calculated seismic parameters K_{cj} , W_j in the seismic cycles of strong earthquakes for SS Sakhalin with $M_{th} = 6.2$. Calculations for earthquakes 4, 5 and 6 were done for two cases of the catalogue with representative M_{min} equal to 4.0 and to 5.0 (those parameters are indicated in brackets). Below, parameters ϕ° and λ° are latitude and longitude, respectively (in degrees). The symbol (*) below implies a hypothetical value.

j	Data	ϕ°	λ°	K_s	M_s	K_{cj}	W_j	(K_{cj})	(W_j)	Place
1	1907 January 19	50.50	141.40	15.3	6.6	14.19*	15.75*	—	—	Aleksandrovsk
2	1924 March 15	49.30	142.00	15.5	6.8	14.18	16.15	—	—	Uglegorsk
3	1971 September 5	46.25	141.20	16.3	7.5	15.24	17.67	—	—	Moneron
4	1995 May 27	52.64	142.87	15.9	7.2	14.69	17.67	14.67	16.92	Neftegorsk
5	2000 August 27	52.64	142.87	15.5	6.8	14.11	14.07	14.07	15.82	Uglegorsk
6	2012 November 1			>7.1	14.94	16.75	14.87	16.69		C or D zone

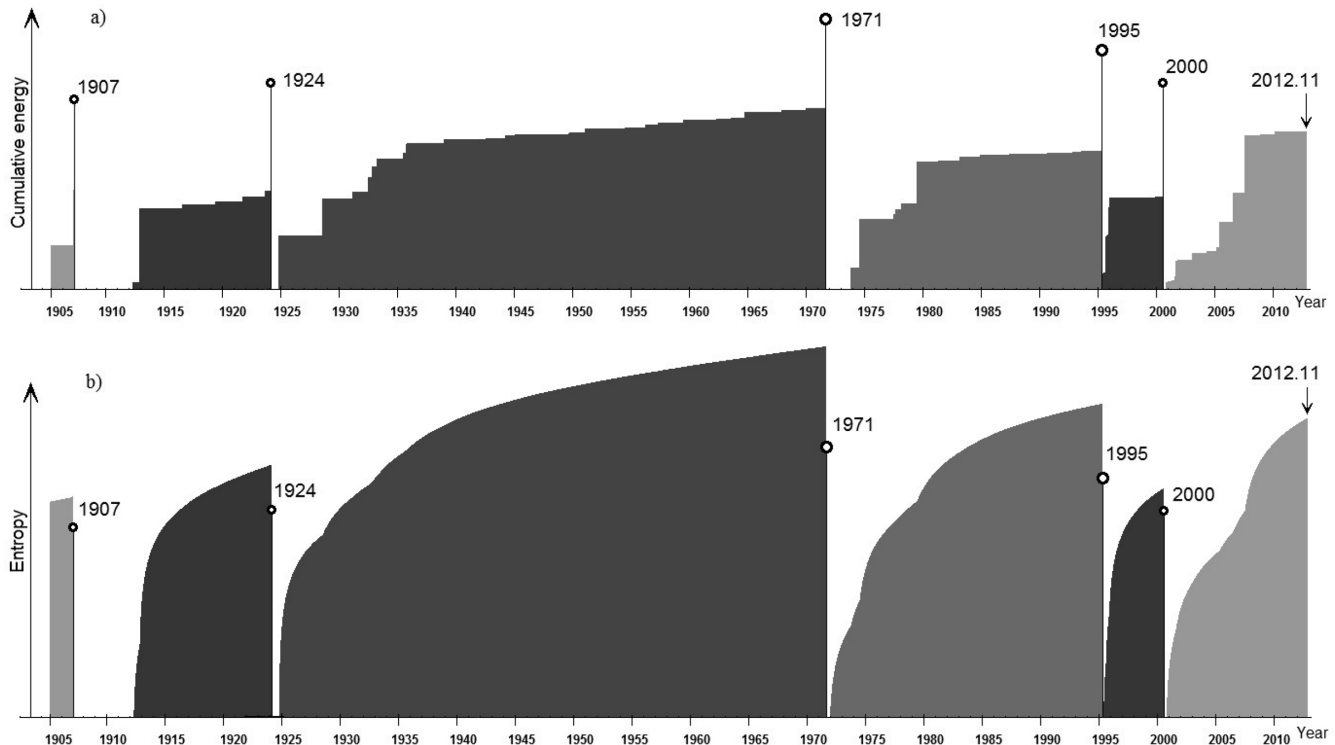


Figure A2. Graphs of cumulative energy (a) and entropy (b) in the seismic cycles of SS Sakhalin. At the end of seismic cycles, strong earthquakes are shown.

Studying the configuration of trajectories, tectonics and focal mechanisms allows for a better interpretation of details of local sections of the attractor, as well as other factors that are not considered here.

Let us also estimate the influence of the inhomogeneity among lower-level magnitudes in the earthquake catalogue upon calculated results. We can assume that, for the catalogue of Sakhalin Island from 1909 to 1973, representative earthquakes start with $M = 5.0$, and that from 1973 to 2012, they start with $M = 4.0$. Table A1 shows calculated K_{sj} and W_j values for the two cases seismic cycles of 1995, 2000 and the incomplete cycle of 2012, where representative M_{min} equals 4.0 and 5.0, respectively. For these cycles, changes in ΔK_c , $\Delta E_c/E_c$, $\Delta M_c/M_c$ and ΔW are shown in Table A2.

Thus, increasing the number of indicator earthquakes by adding new data to the catalogue of weak earthquakes has almost no effect on the accuracy of the results. Therefore, for forecasts in time windows of more than 3 months, they can be discarded. The large indicator earthquake with $M \geq 5.0$ is the main contributor to the cumulative energy (close to 90 per cent) and plays a crucial role in the construction of an attractor and in the preparation of strong earthquakes. The energy and entropy cost contribution of large earthquakes can be even higher. This increases the reliability of the universal law (A2). Within the most significant indicator earthquakes ($M = 5.0\text{--}5.5$),

errors of 0.1 magnitude lead to small changes in the calculations ($\Delta K = 0.04\text{--}0.17$ per cent and $\Delta W = 0.07\text{--}0.18$ per cent). These insignificant changes mainly involve the third decimal place and are less than 1/10 the size of the circles in Fig. A3. They do not qualitatively affect the results of the regression equation.

Now we illustrate how to retrospectively predict the Uglegorsk earthquake (2000) based on the trajectory diagram discussed schematically in Fig. 9. For the prediction, we have to use an attractor (A1) built before 2000 (Akopian 1998a). For example, before the Uglegorsk earthquake, in August 2000, the trajectory had coordinates ($K_{t_m} = 14.109$, $W_{t_m} = 15.862$). The trajectory is located above the attractor. Assuming that after $t > t_m$ there were no indicator earthquakes in the system,

$$E_c(t) = E_c(t_m) \quad \text{for } t > t_m, \quad (\text{A3})$$

the entropy at a later time can be found by using formula eq. (5) in Akopian (1995b):

$$W(t_m + m) = \log\{S(t_m) + mE_c(t_m)\}, \quad (\text{A4})$$

where $m = \Delta t/\delta t = 1, 2, 3, \dots$ is a counter of the number of months since current time t_m . Solving this equation together with linear eq. (22), we find the time when the path trajectory intersects

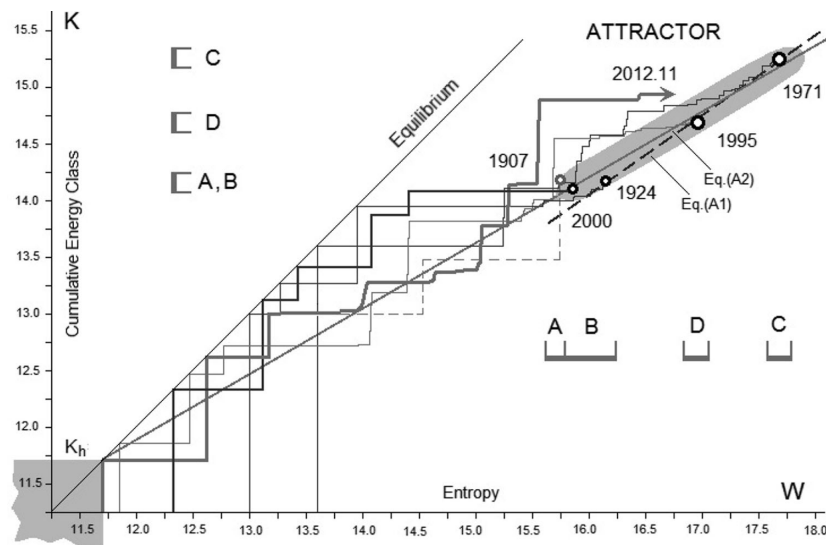


Figure A3. The trajectory diagram and attractor for SS Sakhalin. The trajectory of pending cycle (2012 November) shows a thick line. Eqs (A1) and (A2) are the regression lines by three points in 1995 and by five points in 2000, respectively. Shown: the critical areas of the attractor A, B, C and D with respect to entropy and to cumulative energy class; the area of equilibrium near the origin ($K_h = 11.7$); and the hypothetical trajectory for the earthquake of 1907 (dotted step line).

Table A2. Change of parameters in seismic cycles as the lower threshold magnitude of catalogue representativeness decreases from 5.0 to 4.0. M_c is the magnitude of a hypothetical indicator earthquake with cumulative energy E_c .

Seismic cycle	ΔK_c	$\Delta E_c/E_c$	M_c	$\Delta M_c/M_c$	ΔW
1971.10–1995.05	+ 0.025 (0.17 per cent)	5.9 per cent	6.1	0.23 per cent	+ 0.016 (0.09 per cent)
1995.06–2000.08	+ 0.041 (0.29 per cent)	10.9 per cent	5.6	0.41 per cent	+ 0.039 (0.25 per cent)
2000.09–2012.11	+ 0.072 (0.48 per cent)	11.2 per cent	6.3	0.63 per cent	+ 0.064 (0.38 per cent)

with the regression line (attractor):

$$m = 10^{(W_{lm} - K_{lm})} \left[10^{\frac{(K_{lm} - b)}{a}} - W_{lm} - 1 \right]. \quad (\text{A5})$$

Substituting the values of the trajectory coordinates and using the coefficients a, b from (A1), we find $m = 32$ months, that is, 2 yr and 8 months. The dangerous period for culmination in a strong earthquake was proposed to be 2003 March. Considering possible missing data in the catalogue before 1924, one can predict the dangerous period to be from 2001 August to 2003 March. It therefore appears to be a rather poor prediction. However, if the calculation of the regression eq. (A1) also includes the hypothetical point of instability in 1907, the dangerous period includes 2000 July–September, when the strong earthquake actually occurred. The location is also well predicted, near the earthquake of 1924, in area B. The greater the number of seismic cycles, the better the prognosis. After each completed cycle, the results become more (statistically) accurate and, therefore, the attractor is refined.

Currently, as shown in Fig. A3, the track is located high above the attractor. Such situation has occurred after the Nevelsk earthquake in 2007 August 2, with magnitude $M = 6.1$, which we ranked as the indicator earthquake. There is some ambiguity in the choice of threshold magnitude $M_{th} = 6.2$, which is in the interval between the strongest indicator earthquake (6.1) and the weakest strong earthquake (6.6). However, over time, as this interval fills with earthquakes, the magnitude of the threshold becomes more specific. According to formula (A5), using data from Table A1, we estimate that the next strong earthquake (magnitude $M > 7.1$) will occur later than $m = 161$ months, or by 2026, in zone D or C. However, practical monitoring of Sakhalin simultaneously in the hierarchy of

the SS, in the North (zone D) and South (areas A, B and C) subsystems, where $M_{th} = 5.6$, allows multilevel control of seismicity and improves the accuracy of forecasts.

Regarding SS Sakhalin, see also Fig. 11 and Section 4.2, Fig. A4 shows the cumulative frequency–magnitude relation of SS Sakhalin in four time intervals: 1971–2012, two complete seismic cycles (1971–1995, 1995–2000) and one unfinished cycle (2000–2012). The calculations were performed for the catalogue with $M_{min} = 2.8$ and magnitude window $\Delta M = 0.2$. By introducing the average number of earthquakes, and writing GR regression lines in the form of $\log(N/T) = \hat{a} - \hat{b}M$, then, for selected four time intervals of SS Sakhalin, the \hat{b} value is equal to 0.42, 0.36, 0.40, 0.42 and \hat{a} equals 1.41, 0.94, 1.62, 1.61, respectively. The low values of these parameters result from the slow rate of tectonic processes in SS Sakhalin. Indicator earthquakes in the range $4.3 < M < 6.2$ are not correlated with the GR empirical law (calculated in accordance with the parameters of SS Sakhalin) and occur randomly. These indicator earthquakes provide the main contribution to the cumulative energy (more than 99 per cent). Thus, for SS Sakhalin, with threshold magnitude $M_{th} = 6.2$, indicator earthquakes with a lower threshold ($M_h = 4.3$) play a crucial role in the preparation of ensemble of strong earthquakes.

APPENDIX B: SEISMIC SYSTEMS ON THE MAP

The geographical locations of SSs in Table 2 are presented here. The configurations, epicentres of indicator earthquakes, and zones of instability (for strong earthquakes in ensemble) of these systems

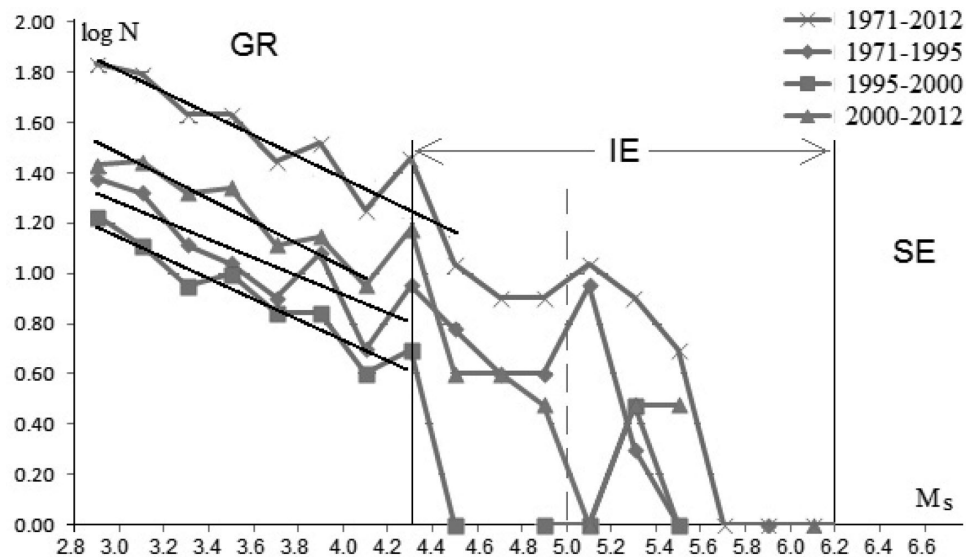


Figure A4. The Gutenberg–Richter law calculated in accordance with the parameters of SS Sakhalin. Events are considered in four time intervals for the catalogue beginning with $M_{\min} = 2.8$ and magnitude window $\Delta M = 0.2$. In the range $4.3 < M < 6.2$, indicator earthquakes are uncorrelated and occur randomly.

are given on the map (Figs B1–B9). The areas of instability for SS in continental convergence and transform fault zones are indicated by rectangles, and the subduction zones are indicated by oval lines.

B1 The SS Japan and Mega Japan (MJ)

Fig. B1 shows the configuration of the SS Japan and indicator earthquakes with magnitudes $M \geq 5.5$. The configuration of the SS MJ coincides with the SS Japan but differs by threshold magnitude. These systems have a depth of 100 km and describe a dynamic behaviour and time evolution of the complex (seismically) active structures of the lithosphere in the area of Honshu, Shikoku and

Kyushu Islands, formed by the interaction of the Pacific, Philippine and Eurasia plates. Zones of mega earthquakes 1933, 1946 and the last catastrophic earthquake Tohoku 2011, whose preparation well described in the SS MJ, are also shown in Fig. B2. The mean recurrence interval of strong earthquakes in the SS Japan, after completing 14 seismic cycles, is equal to 7.3 yr, while in the SS MJ the average periodicity, after three seismic cycles since 1896, is equal to 38.3 yr.

B2 The SS Mega Chile

Fig. B2 shows the configuration of the SS Mega Chile which extends along the western coast of South America, and indicator earthquakes

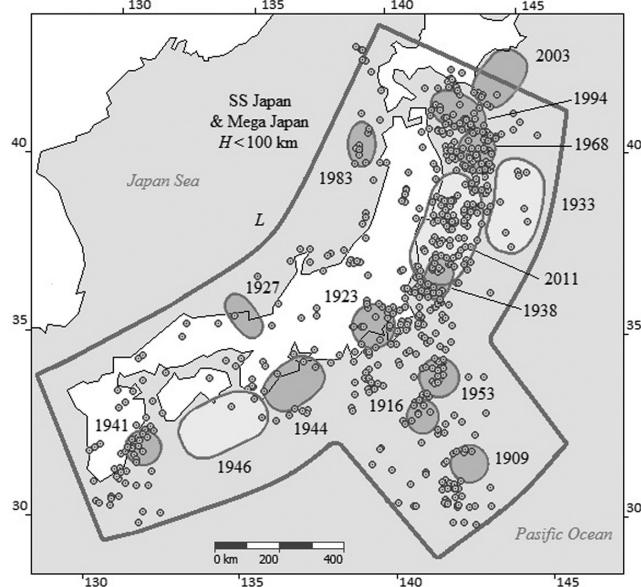


Figure B1. Configuration L of the SS Japan and Mega Japan. The boundaries of these two systems are the same. The zones of strong earthquakes are indicated by shaded oval (contour) lines. The unshaded ovals represent the zones of mega earthquakes. The indicator earthquakes are marked by smaller shaded circles. In each zone of instability the specified years are the implementation dates of strong earthquakes.

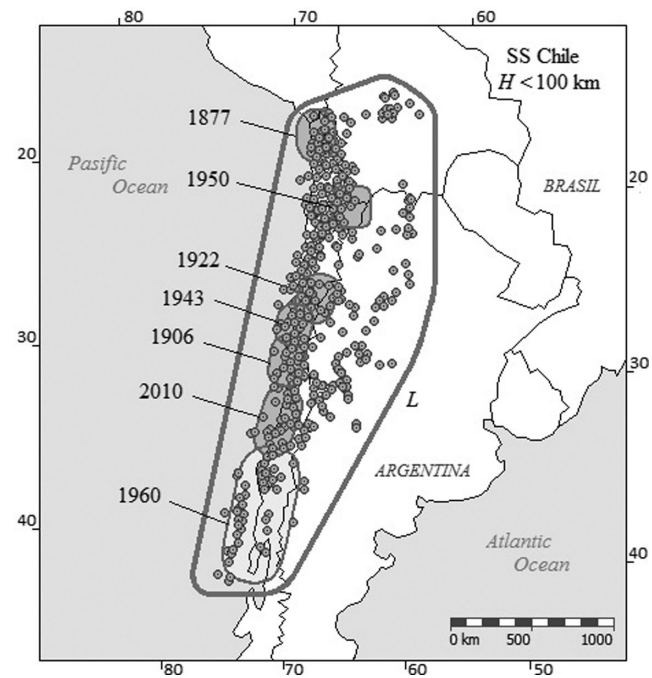


Figure B2. Configuration L of SS Mega Chile. The notations and curves mean the same as in Fig. B1.

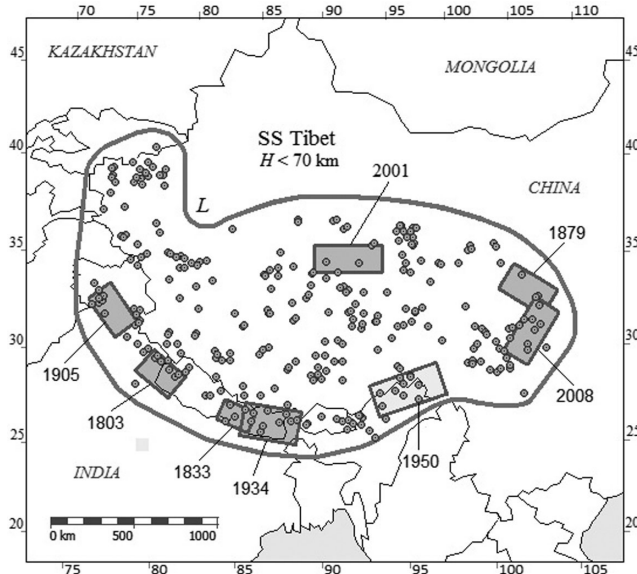


Figure B3. Configuration L of SS Tibet. Notations are the same as in Fig. B1, but zones of strong earthquakes are indicated by shaded rectangles.

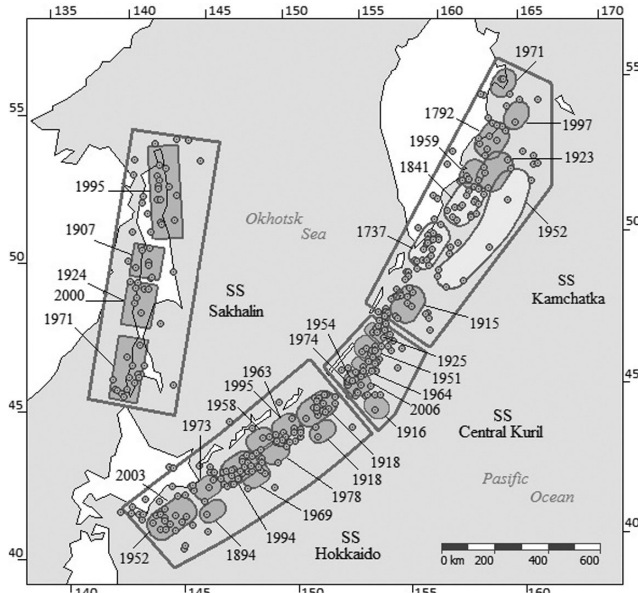


Figure B4. Configurations of the SS Kamchatka, Central Kuril, Hokkaido and Sakhalin. The notations and curves mean the same as in Fig. B1.

with magnitudes $M \geq 5.5$. This system has a depth of 100 km, and is responsible for the ensemble of strong earthquakes in the area of interaction between the Nazca and South America plates. The Nazca Plate moving eastward plunges beneath the South American Plate. In this system, the strongest earthquake with $M = 9.5$ since the beginning of the twentieth century occurred on 1960 May 22. The last strong earthquake ensemble (Concepcion-Valparaiso) occurred on 2010 February 27. The mean recurrence interval of strong earthquakes in the SS Mega Chile, after completing five seismic cycles since 1906, is equal to 20.8 yr.

B3 The SS Tibet

Fig. B3 shows the configuration of the SS Tibet, and indicator earthquakes with magnitudes $M \geq 5.5$. This system has a depth

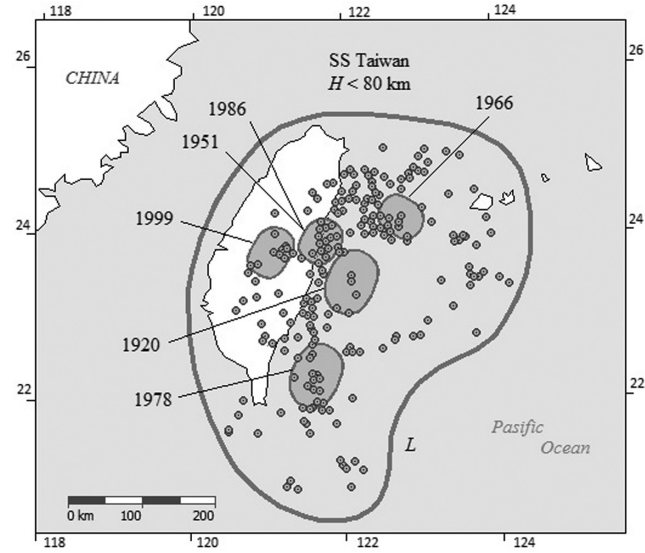


Figure B5. Configuration L of SS Taiwan. The notations and curves mean the same as in Fig. B1.

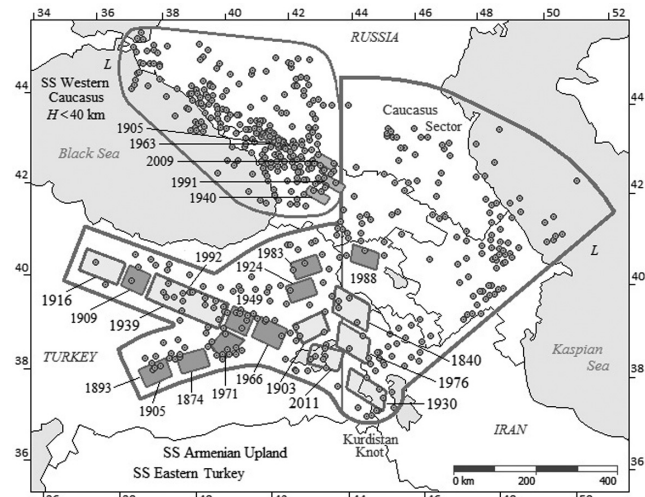


Figure B6. Configurations of the SS Eastern Turkey, Armenian Upland, and Western Caucasus. Caucasus Sector and its top Kurdistan Knot are also shown. Notations are the same as in Fig. B1, but the zones of strong earthquakes are indicated by shaded rectangles.

of 70 km, and describes the dynamics in an ensemble of strong earthquakes on the Tibetan Plateau caused by collisions between the Indian and Eurasian plates. As a result of such collisions, the Tibetan Plateau has been formed, due to the complex lithospheric deformations in the form of stretches in the northern direction for 1600 km, and 2500 km along the east and west. The system includes Tibet within China, the Himalayas (NE of India, Nepal, Bhutan) and north of Bangladesh. The mean recurrence interval of strong earthquakes in the SS Tibet, after completing seven seismic cycles since 1833, is equal to 25.6 yr. The last strong earthquake in the ensemble has happened recently, on 2008 May 12 in China, Sichuan. The earthquake (Assam) in 1950 in NE India is a mega earthquake.

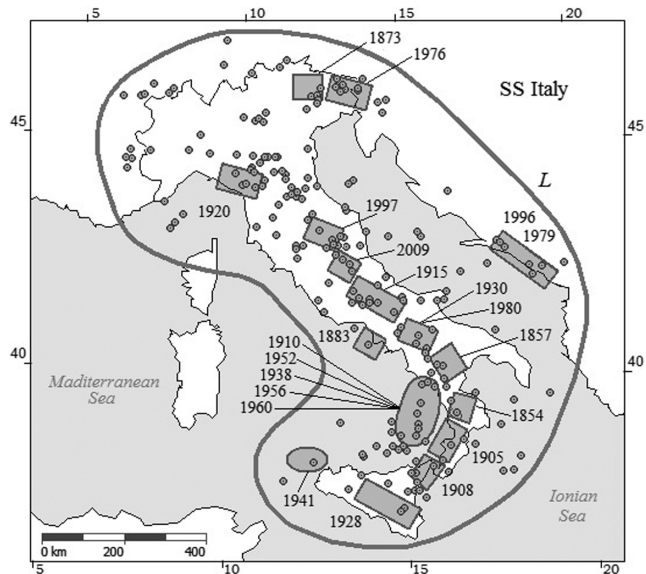


Figure B7. Configuration *L* of the SS Italy. Notations are the same as in Fig. B1. Zones of shallow strong earthquakes are indicated by shaded rectangles.

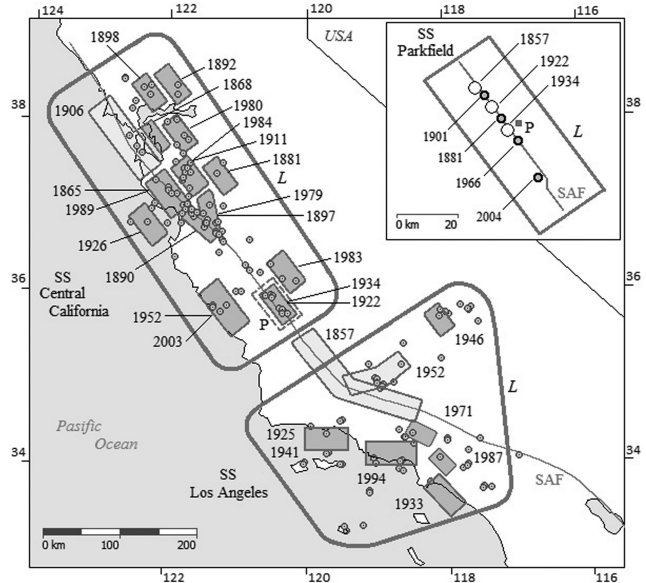


Figure B8. Configurations *L* of the SS Central California, Los Angeles and Parkfield. Notations are the same as in Fig. B1, but zones of strong earthquakes are indicated by shaded rectangles. The legend shows the SS Parkfield in a dashed rectangle *P*. Here open circles denote the strong earthquakes in the SS Central California, while the shaded ones are those in the SS Parkfield.

B4 The SS Kamchatka, Central Kuril (CK), Hokkaido and Sakhalin

Fig. B4 shows the configurations of these systems, and indicator earthquakes (Kamchatka $M \geq 6.0$, CK $M \geq 5.8$, Hokkaido $M \geq 6.6$). These systems have a depth of 70 km, and include ensembles of strong earthquakes that reflect the dynamics of interaction between the Eurasian and Pacific plates. In this region, the Pacific Plate subducts beneath the Okhotsk Plate at the Kuril-Kamchatka Trench and descends progressively deeper northwest, remaining seismically active up to a depth of about 680 km. The mean recurrence interval of strong earthquakes, after completing six seismic cycles

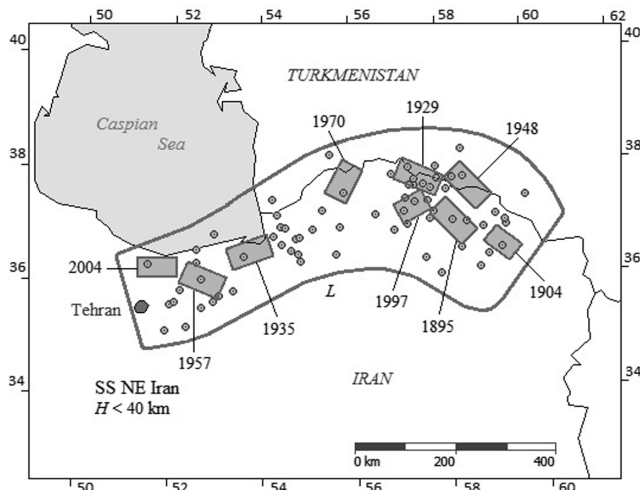


Figure B9. Configuration *L* of the SS NE Iran. Notations are the same as in Fig. B1, but zones of strong earthquakes are indicated by shaded rectangles.

since 1899, in the SS Kamchatka is equal to 28.8 yr. In the SS CK the mean recurrence interval of strong earthquakes, after completing 6 seismic cycles since 1916, is equal to 15 yr. In the SS Hokkaido, the average periodicity of strong earthquakes, after completing 10 seismic cycles since 1900, is equal to 10.3 yr. The last strong earthquake in the SS Kamchatka (Kronotsk) was on 1997 December 5. In the SS CK, the last strong earthquake was on 2006 November 15, and in the SS Hokkaido, the last strong earthquake (Tokachi Oki) was on 2003 September 25. The SS CK, with relatively small size and threshold magnitude, plays an important role in coordinating and linking the active processes between the SS Kamchatka and the SS Hokkaido.

B5 The SS Taiwan

Fig. B5 shows the configuration and indicator earthquakes in the SS Taiwan with magnitudes $M \geq 5.5$. The system has a depth of 80 km, and describes the dynamics in an ensemble of strong earthquakes in the area of interaction between the Eurasian and Philippine Sea plates. The SS Taiwan includes the Taiwan Island which is compressed in an east–west direction between these plates. The average periodicity of strong earthquakes in the SS Taiwan, after completing of six seismic cycles since 1901, is equal to 16.3 yr. The last extraordinary catastrophic earthquake in the system (Chi-Chi) took place on 1999 September 20.

B6 The SS Eastern Turkey (ET), Armenian Upland (AU) and Western Caucasus (WC)

Fig. B6 shows the configurations of these systems, and indicator earthquakes with $M \geq 5.0$ (in the WC—with $M \geq 4.0$). The system boundaries of AU and ET are the same, while their threshold magnitudes are different. These systems have a depth of 40 km, and include ensembles of strong earthquakes that reflect the dynamics of the complex plate-block structure formed by the wedging and (counterclockwise) rotation of the Arabian Plate against the Eurasian Plate. Regional stresses in the Tauro-Caucasus region, primarily concentrated in the Kurdistan Knot are redistributed to the Caucasian Sector in radial directions before reaching the northern foothills of the Caucasus, causing seismic activity. According to this model, activation of the indicator earthquakes in the Caucasian

sector can serve as an indicator of the rate of movement of the Arabian Plate and presage catastrophic earthquakes in the AU, ET and WC. The mean recurrence interval of strong earthquakes in the SS ET, after completing six seismic cycles since 1830, is equal to 30.3 yr; in the SS AU, the mean recurrence interval of strong earthquakes, after completing 16 seismic cycles since 1830, is equal to 11.4 yr; in the SS WC the mean recurrence interval of strong earthquakes, after completing five seismic cycles since 1905, is equal to 21.4 yr. The last strong earthquake in systems AU and ET occurred on 2011 October 23 (Lake Van); in the SS WC, 2009 September 7 (northern Georgia).

B7 The SS Italy

Fig. B7 shows the configuration, and indicator earthquakes with $M \geq 5.0$. The SS Italy describes the dynamics of the region seismotectonics, due to the interactions extended between far to the north of the Adriatic Cape of the African Plate and the Eurasian Plate. The ensemble of strong earthquakes in Italy is the result of a collective seismic response to the northern movement of the Adriatic and the African plates in relation to the Eurasian Plate, and the counter-clockwise rotation of the Adriatic Plate in relation to the African Plate. This system is specified by the existence of the subduction zone to the south of Italy (SE Tyrrhenian), accompanied by deep-focus seismicity (including 1910, 1938, 1952, 1956 and 1960 strong earthquakes in the ensemble) and active volcanism. The depth of the SS Italy varies from 60 km in the north to 500 km in the south and includes a miniature subduction zone in SE Tyrrhenian. The mean recurrence interval of strong earthquakes in the SS Italy, after completing 19 seismic cycles since 1854, is equal to 8.2 yr. The last strong earthquake (L'Aquila) occurred on 2009 April 6.

B8 SS Central California (CC), Los Angeles (LA) and Parkfield (P)

Fig. B8 shows the configurations of these systems, and indicator earthquakes with $M \geq 5.0$. These systems have a depth of 40 km, and are located in the contact zone between the Pacific and North

American plates in central and south California. They include ensembles of strong earthquakes, reflecting the dynamics of the different segments of the SAF and its branches. The SS CC indicates that there is a close interaction between the Parkfield segment of the SAF and its branched faults in the San Francisco Bay area (separated by a creep zone) for a collective seismic response to external compression. The threshold magnitude of the SS CC ($M_{th} = 6.0$) divides the sequence of Parkfield earthquakes by magnitude into two types: strong earthquakes (1857, 1922 and 1934 shocks), and indicator earthquakes (1881, 1901, 1966 and 2004 shocks). The SS CC is responsible for the preparation of the Parkfield earthquakes in 1857, 1922, 1934 and the small SS Parkfield is responsible for earthquakes in 1881, 1901, 1966 and 2004. The mean recurrence interval of strong earthquakes in the SS CC, after completing 18 seismic cycles since 1865, is equal to 8.2 yr; in Parkfield, the average periodicity, after completing six seismic cycles since 1857, is equal to 24.5 yr. The last strong earthquake in the SS CC (San Simeon) occurred on 2003 December 22 and in the SS Parkfield on 2004 September 28. The SS LA indicates that there is a correlation between the seismicity of the Carrizo Plain segment of the SAF, White Wolf fault zone and fault systems in the Los Angeles area. The mean recurrence interval of strong earthquakes in the SS LA, after completing eight seismic cycles since 1902, is equal to 11.5 yr. The last strong earthquake in the SS LA (Northridge) occurred on 1994 January 17. The preparedness of the mega earthquakes in these systems (1857 Fort Tejon, 1906 San Francisco and 1952 Kern County) are well described in the united mega system, which is not discussed here.

B9 The SS NE Iran

Fig. B9 shows the configuration L , and indicator earthquakes with $M \geq 5.0$. The SS NE Iran with a depth of 40 km describes the dynamics at the junction of the Iranian and the South Caspian plates. The Iranian Plate from the south is compressed by the Lut Plate. The mean recurrence interval of strong earthquakes in the SS NE Iran, after completing seven seismic cycles since 1904, is equal to 15.4 yr. The current seismic cycle started in 2004.